THESIS

DETERMINING THE DIFFERENCE BETWEEN MEASURED AND CALCULATED DOSE TO CANINE ORAL MUCOSA DURING STEREOTACTIC RADIATION THERAPY USING GAFCHROMIC™ FILM

Submitted by

Ward Mazyad

Department of Environmental and Radiological Health Sciences

In partial fulfillment of the requirements

For the Degree of Master of Science

Colorado State University

Fort Collins, Colorado

Fall 2011

Master's Committee:

Advisor: Susan LaRue

James Custis
Joseph Harmon
Brian Kavanagh
Katharine Lunn

ABSTRACT

DETERMINING THE DIFFERENCE BETWEEN MEASURED AND CALCULATED DOSE TO CANINE ORAL MUCOSA DURING STEREOTACTIC RADIATION THERAPY USING GAFCHROMIC™ FILM

Among the therapeutic approaches available to manage canine nasal tumors, radiation therapy is considered the standard of care for achieving improved quality of life and overall survival time for these patients. Long-term local tumor control remains the goal for many radiation therapy protocols applied to patients with canine nasal tumors. Stereotactic radiation therapy (SRT), utilized by Colorado State University Animal Cancer Center (CSU-ACC), delivers maximum dose to the tumor volume, while preferentially sparing the surrounding normal structures. When treating dogs with nasal SRT, there is uncertainty with regard to the actual dose delivered to the oral mucosa due to the anatomical proximity of the tumor and the inherent error of most algorithms in calculating doses at air-tissue interfaces. A canine head phantom, dogs with spontaneously-occurring tumors, and the Gafchromic EBT film analysis system were utilized to measure radiation dose. Further comparison between measured film dose and dose calculated by the Varian Eclipse inverse planning algorithm was conducted. The results from this study demonstrate the high variability of the Analytical Anisotropic Algorithm (AAA) in

calculating doses for this particular geometry. The high degree of variability results in uncertainty with regard to the prediction of delivered dose. The differences between measured and calculated doses in both the phantom (mean difference of 104 cGy per fraction, p-value of <0.0001) and the dogs (mean difference of 74 cGy per fraction, p-value of 4.2×10^{-5}), suggest that the AAA underestimates the dose delivered to oral mucosa of dogs treated with SRT to manage their nasal tumors. Based upon a dose prescription of 10 Gy tumor dose per fraction in this population of dogs, an oral mucosa dose range of 3.5-6.5 Gy per fraction was measured in 88% of the cases, this range might be considered by clinicians in an effort to estimate the dose delivered to the oral mucosa while treating canine nasal tumors with SRT.

ACKNOWLEGMENTS

First I would like to thank my family. Mom and dad, I thank God I have you beside me. Thank you for the love and support you provided me and for never letting me feel lonely. My sister, Alyaa, thanks for all the times you made me laugh to alleviate my stress. I always miss chatting with you, my soul mate. My sisters and brother, back at home, even when you are so far away you are always in my heart and mind. Your love and care helped me through difficult times. Sama, my lovely niece, I'll always love and miss you, my baby.

I would like to thank my advisor, Dr. La Rue. Your creative ideas helped me get past many obstacles. Your joyous soul inspired me to surpass difficulties and always do my best.

To Dr. Custis, words can never describe my gratitude and appreciation for your endless help through the research and writing process. Your support was the light that guided my way when I was desperate. I would never be able to carry on without your help.

To Dr. Harmon, I learned a lot from you during the few months we were working together to design the project. I felt sorry after your departure for losing a great teacher and mentor. However you were always available to help. Thank you for your time and support.

A special thank you to Dr. Pinder, it is always interesting and fun to work with you. Sorry for all the late Friday afternoon talks. Your enthusiasm and encouragement were invaluable to my success. I will always remember what you told me about the dementors.

To Lynn, Mike, Channa and Frank, I would like to thank you all for the help and support you provided me. Lynn, I appreciated your texting me whenever you knew of a new patient. Mike, thank you for always being willing to help in answering my questions. Channa, I am sorry for all the biting you endured while helping me place the film. Frank, thank you for spending your breaks with me, helping me irradiate my phantom.

To Hanaa, Arwa, and Fatima, I am going to miss you a lot my dearest friends. I will miss our Friday nights. Hanaa, thank you for all the laughs and the good times we spent together, I will never forget your Turkish coffee. Arwa, you are such a wonderful friend. You always understood me, helped me, and were there for me when I needed you. Fatima, I met a lot of people and made a lot of friends but I would never find as caring and as loving a heart as yours. You will always be in my heart dear.

To my friend Liz, your love and support made you like a family to me. I will miss joining you and your wonderful family on Thanksgiving and Easter occasions. I will also miss all the interesting conversations we had. God bless you my dear and bless your loving heart.

Finally I would like to thank my phantom, Franken Dog. Sorry for all the radiation I gave you. I know that no one else could stand it. I love the scar you made on my finger. It will always remind me of you and of every day of the best two years in my life.

LIST OF TABLES

LIST OF FIGURES

TABLE OF CONTENTS

CHAPTER ONE

INTRODUCTION

1.1 Introduction

Due to the locally invasive and aggressive behavior of canine nasal tumors, achieving long-term local tumor control remains the goal of any definitive therapy.[1] Many treatment modalities have been pursued in an effort to extend the overall survival times and improve the quality of life of dogs affected by nasal tumors. Overall, surgery, chemotherapy, immunotherapy, and cryosurgery have failed to improve the clinical outcome in patients with canine nasal tumors over untreated dogs.[1,4,7,13,15] Radiation therapy, alone or combined with other therapy, is the only modality proven to improve patients outcome with regard to overall survival and quality of life.[1,4,5,7,13,15] Many radiation therapy protocols have been examined in an effort to determine the best approach to canine nasal tumors (Table 1.1).[1,11-20,41] There is appreciable interinstitutional variation among veterinary radiation therapy protocols based upon time, dose, and fractionation.

Stereotactic Radiation Therapy (SRT) has been utilized by Colorado State University-Animal Cancer Center (CSU-ACC) to treat canine nasal tumors. SRT uses advances in immobilization techniques, image-guided radiation therapy (IGRT), and multi-leaf collimators to modify the intensity of delivered dose, thus

Table 1.1 Summary of selected articles on treatment of canine nasal tumors with radiation (1)

	Adams *et al.*[13]	Northrup *et al.*[18]	Theón *et al.*[19]	McEntee *et al.*[16]	Adams *et al.* [12]	Lane *et al.*[15]	Adams *et al.*[11]	Adams *et al.*[11] (historic controls)	Mellanby *et al.*[17]	Hunley *et al.*[14]	Lawrence *et al.*[41]	Custis *et al.*[20]
Number of dogs	67	42	77	27	21	51	13	40	56	12	31	16
Adjuvant Therapy: *Surgery*	41/67	42/42	21/77*	6/27	None	None	11/13 after RT	None	None	None	None	None
Chemotherapy	None	None	None	None	14/21†	51/51Ω	None	None	None	None	None	None
Survival: *Median(months)*	8.1	7.4	12.6	12.8	14.3	15.8	47.7	19.7	7	14.9	14	12.2
1 year/2 year (%)	38/30	37/17	60/25	59/22	60/36	Not Reported	76/69	68/44	45/15	50/25	Not Reported	Not Reported
Dose (Gy): *Mean*	43											
Median		48	48	41-54	42	54	42	42	36	54	42	29.1
Number of fractions	5-10	12	12	10-12	9-10	18	10	10	4	18	10	3
Overall treatment time(days)	22 -28	26	26	26	11-13	24	12	12	22	40	12	3
Radiation source	Variable	Orthovoltage (low energy)	Cobalt	Cobalt	Cobalt	6-MV linear accelerat –or	Cobalt	Cobalt	4-MV linear accelerat -or	6-MV linear accelerat -or	6-MV linear accelerat -or	6-MV linear accelerat -or

* *Measurable diseases remained in all dogs after the surgical procedure.*

†*Immunotherapy was given using liposome-encapsulated MTP-PE.*

Ω *A slow release formulation of cispaltin was given as chemotherapy.*

RT, Radiation therapy.

targeting the dose to the tumor volume while sparing the surrounding normal tissues.[20,22] SRT was initially utilized in humans to treat primary and metastatic brain tumors.[23,24] The concept of giving radiation in large doses in a small number of fractions over a few days raises the concern about the possibility for radiation-induced adverse effects.[22,24] Self-limiting and reversible oral mucositis is frequently seen when radiation is used to manage canine nasal tumors and is observed as early as 2 weeks into treatment. Late effects on the oral cavity are dose limiting and include osteoradionecrosis and oro-nasal fistula.[6]

Within the Varian Eclipse inverse planning algorithm, there is inherent uncertainty associated with the predicted dose within the first 2 mm of an air-tissue interface.[26,27] Radiation oncologists must be cautious in sparing the oral mucosa to avoid complications. The aim of this work is to estimate the difference, if any, between measured and calculated dose to the portion of the oral mucosa in anatomical proximity to the nasal cavity. We hypothesize that the difference between measured and calculated dose will be statistically significant. Specifically, we expect the measured dose will be higher than calculated dose. To test this hypothesis, the radiochromic film system will be verified, a head phantom will be constructed, and both the phantom and dogs with spontaneously-occurred tumors irradiation will be examined to compare the doses measured by Gafchromic EBT film to those calculated by the planning software.

1.2 Canine Nasal Tumors

1.2A Background and Treatment Modalities

Canine nasal tumors, the 5th most common type of neoplasia treated by external beam irradiation,[8,10] account for only 1-2% of all tumors in dogs These tumors are malignant in 80% of the cases.[1-4] Carcinomas, most commonly adenocarcinoma, accounting for two-thirds of all nasal tumors, are more frequently seen than sarcomas such as chondrosarcoma, osteosarcoma, and fibrosarcoma.[1-3,5,6] The median age of affected dogs at presentation is approximately 10 years old, however the observed range is wide.[1,2,4,6] Dogs with sarcomas may present at a younger age than dogs with carcinomas.[3,4] Some variables have been studied as potential risk factors for developing canine nasal tumors. Indoor coal or kerosene combustion have been correlated to the development of a canine nasal tumors.[1,6,70] Sex, breed, and tobacco exposure are factors that showed inconsistent correlation to outcome in a number of studies.[1,6,70,71] In most cases, a definitive diagnosis of nasal neoplasia is not obtained until 3-4 months after the onset of clinical signs.[1,2] The slow and insidious behavior of the tumor results in the formation of a space-occupying mass as well as invasion and destruction of adjacent structures, giving rise to the majority of the presenting clinical findings[1,3] such as: epistaxis, unilateral or bilateral nasal discharge (mucopurulent or serosanguineous), air flow obstruction, sneezing, facial deformity, dyspnea, or ocular discharge. Neurologic signs such as seizures, behavioral changes, circling, visual deficits or ataxia are possible if the tumor invades through the cribriform plate and into the brain.[1-7]

Non-neoplastic disease processes can be present with similar signs and symptoms to nasal tumors especially early in the tumor course. Rhinitis (chronic bacterial, viral, or fungal such as Aspergillosis), foreign body impaction, periodontal abscess, and trauma are example of conditions that may resemble the presentation of nasal tumors.[1-4,6]

Radiographs and computed tomography (CT) allow for evaluation of the extent of local disease. However, definitive diagnosis is based on the histological examination of an adequate tissue sample taken from the tumor.[1-6] The well-known tendency of nasal tumors to locally invade rather than metastasize, makes controlling the local disease the main goal of treatment.[1,2] Metastasis of canine nasal tumors is usually slow, late, and uncommon, and more frequent in tumors of epithelial origin than in those of mesenchymal origin.[3] Common sites of metastasis are regional lymph nodes, lungs, and brain. Other less frequent sites include bone, liver, adrenal glands, and testicles.[1-4,6]

The median survival time for untreated dogs is 3-5 months.[4,5,9,13] Surgical management has shown to be associated with acute and chronic morbidity, high recurrence rate, and no appreciable survival benefit when compared to untreated patients.[59-63] Surgery is indicated to manage nasal tumors only when combined with radiation therapy.[11,21] The effectiveness of chemotherapy in treating canine nasal tumors is not well supported.[21,64,65] The combination of radiation therapy with slow-release cisplatin showed an improved median survival time over control group treated with radiation only.[15,66] Given the low metastatic rate of canine nasal

tumors, most patients will succumb to manifestations of the local disease process such as local tumor progression, recurrence, or decreased quality of life.[1,7]

1.2B Radiation Treatment of Nasal Tumors: Protocols and Adverse Effects

Radiation therapy is considered to be the standard of care in managing nasal tumors, and is included in any curative-intent treatment protocol.[1,21] Anatomical complexity, geometrical inconsistency, and proximity to sensitive and vital organs are all factors that must be considered during the planning and delivery of radiation therapy for nasal tumors.

Acute and chronic adverse effects can occur following irradiation.[21] Acute side effects involve rapidly dividing tissues such as skin, mucosa, and hair. These effects are usually appreciated one to two weeks after the onset of therapy and subside within two to eight weeks after completion. Oral antibiotics, anti-inflammatories, analgesics, and supportive care can be used to manage acute effects. Late side effects, following radiation therapy, are seen in slowly-dividing organs such as nervous tissues and lenses of the eyes. These effects take months to years to develop and have to be prevented since they tend to be irreversible[1,29-31] (table 1.2).[14,40] Total radiation dose is directly proportional to the severity of both acute and late adverse effects. Extending the treatment over a longer period of time preferentially spares early responding tissues because of their rapid repair, while smaller dose per fraction favors sparing late responding organs.[29,30]

Table 1.2 Veterinary Radiation Therapy Oncology Group (VRTOG) acute and late radiation morbidity scoring schemes for eye, skin, central nervous system (CNS), and oral cavity (14,40)

Organ/Tissue	Acute/Late	Grade 0	Grade 1	Grade 2	Grade 3
Eye	Late	None	Asymptomatic cataracts, KCS	Symptomatic cataracts, keratitis, corneal ulceration, minor to moderate glaucoma	Panophthalmitis, blindness, severe glaucoma, retinal detachment
Eye	Acute	No change other baseline	Mild conjunctivitis and/or sclera injection	KCS requiring artificial tears, moderate conjunctivitis or iritis necessitating therapy	Severe Keratitis with corneal ulceration and/or loss of vision, glaucoma
Skin	Acute	No change other baseline	Erythema , dry desquamation, alopecia/epilation	Patchy moist desquamation without edema	Confluent moist desquamation with edema and/or ulceration, necrosis, hemorrhage
Skin/hair	Late	None	Alopecia, hyperpigmentation, leukotrichia	Asymptomatic induration(fibrosis)	Severe induration causing physical impairment, necrosis
CNS	Acute	No change other baseline	Minor neurologic findings not necessitating more than prednisone therapy	neurologic findings necessitating more than prednisone therapy	Serious neurologic impairment such as paralysis, coma, obtunded
CNS	Late	None	Minor neurologic signs not necessitating more than prednisone therapy	neurologic signs necessitating more than prednisone therapy	Seizures, paralysis, coma
Mucous membranes/ oral Caity	Acute	No change other baseline	Injection without mucositis	Patchy mucositis with patient seemingly pain free	Confluent fibrinous mucositis necessitating analgesia, ulceration, necrosis, hemorrhage

KCS=Keratoconjunctivitis sicca

Response to radiation depends on a number of factors such as time, dose, and fractionation of the delivered radiation and size, stage, and histological type of the tumor.[31] Several studies, utilizing radiation alone or in conjugation with other treatment modalities, had been performed, allowing for the comparison of varying fractionation protocols and cumulative total dose with regard to achieving tumor control in dogs with nasal tumors[11-20] (Table 1.1).[1] Long term local tumor control remains elusive for nasal tumor patients, even for those treated with radiation

therapy.[7] Most dogs succumb to tumor recurrence or local disease progression.[1,10,12]

New approaches are now being investigated by many treatment centers to improve local tumor control. Intensity-modulated radiation therapy (IMRT) is one of these methods.[14,21,32] IMRT maximizes the dose delivered to the targeted tumor while minimizing that delivered to nearby normal structures. This approach is used to deliver higher total dose via daily small dose per fraction administration over a period of three to four weeks.[1,14,32] Construction a highly conformal and uniform dose distribution is generated from a number of individual beams with each beam using multiple multi-leaf collimator (static or dynamic MLC) configurations to create a heterogeneous distribution is one of the principles of IMRT.[14,32] Careful delineation of the tumor volume and surrounding vital structures allow for the inverse treatment planning required of IMRT.[14,32] Given the steep dose gradient beyond the target, proper immobilization and positioning of the patient must be maintained to avoid exceeding the known dose constraints to normal tissues or under treating the target.[14,32]

In a recent study,[14] 12 dogs with nasal tumors were treated with an IMRT approach, the median total dose was 54 Gy, and median dose per fraction was 3 Gy in a Monday- Wednesday- Friday schedule. The overall survival time was 14.9 months with 1-year and 2-year survival rates of 50 % and 25 % respectively. This study demonstrates acceptable tumor control with fewer radiation–induced adverse effects for normal tissues outside of the planning target volume (PTV).

The Colorado State University Animal Cancer Center (CSU ACC) has adopted another approach to treating canine patients with nasal tumors. Stereotactic Radiation Therapy (SRT) combines benefits from several advances in the field of radiation therapy; inverse planning, immobilization devices, IGRT (image-guided radiation therapy), and intensity modulation to localize the delivered dose to the tumor while sparing surrounding normal tissues.[20,22] The Varian Trilogy linear accelerator (6 and/ or 10 MV photons) is used to deliver a total dose of 30 Gy in three daily fractions over three consecutive weekdays. This protocol is well tolerated by patients due to fewer anesthetic episodes and less time at the hospital. It is also preferred by owners due to shorter overall treatment time, which is more convenient, and more rapid resolution of the clinical signs. Since surrounding structures are carefully spared during planning and delivery of the dose, tumor control can be improved by reducing the risk of tumor cell repopulation, while taking advantage of fractionation effects on normal tissue repair, tumor reoxygenation, and tumor cell redistribution.[34,35]

In a retrospective study of 16 dogs treated with SRT at CSU ACC, the median overall survival time was 12.3 months and the median disease free interval was 9 months.[20] Acute radiation effects were minimal. Late radiation effects are still being evaluated on dogs that are still alive.

1.3 Oral Mucosa Dose Considerations: Calculation and Measurement Methods

The roof of the oral cavity is composed of three layers: the hard palate, the bony component which separates the nasal cavity from the oral cavity, a relatively

thick mucosal layer and a layer of connective tissue between the hard palate and mucosa.[25] In dogs with nasal tumors, the oral mucosa is contoured just as skin with 2 mm thickness to account for its location. In these patients, the roof of the oral cavity, together with its mucosa, is difficult to spare because of anatomical association with the tumor. Dose to the mucosal layer is the major focus of this study. Excessive dose can cause mucositis, which is generally considered a transient and self-limiting issue. However, consequential late effects to structures such as skin, colon and mucous membranes may be a concern for patients treated with SRT. While mucositis is considered an acute effect, a potential consequential late effect is full thickness ulceration. Ulcerated mucosa over irradiated bone generally will not re-grow leaving bone exposed to the bacterial flora of the oral cavity. This can lead to osteoradionecrosis, which is an irreversible late effect from irradiation that will result in an oronasal fistula. This adversely impacts the patient's quality of life and can lead to weight loss, chronic rhinosinusitis and aspiration pneumonia. .

For most radiation therapy planning software algorithms, there is always more uncertainty in the prediction of dose at air-tissue interfaces in the buildup region. The Varian Eclipse Treatment Planning Software utilizes an AAA algorithm (Analytical Anisotropic Algorithm) to calculate volume doses.[27] This algorithm uses a triple-source model to accurately calculate the dose at a point by superimposing the dose from primary photon, scattered photons, and electrons from contamination sources. The algorithm is based on a Monte Carlo simulation derived scatter kernels model that creates a final dose from superposition and convolution of the primary and secondary photons together with contamination electrons.[26,27,37] When

calculating dose to oral mucosa in a patient with a nasal tumor, the algorithm would apply a simple density scaling of the kernels to the voxels at the interface.[26] Another problem the algorithm has in predicting doses in an inhomogeneous media results from the assumption of straight electrons travelling from the source to destination; divergent scatter of electrons is not well modeled.[26] As a result of the aforementioned limitation within the planning software, there is an uncertainty in predicting the dose within a 2 mm depth in the dose buildup region.[27]

For the purpose of this study, the dosimeter had to meet certain characteristics allowing for measurement of the dose to the oral mucosa in dogs with nasal tumors, while comparing that to the dose calculated by the planning software and the implemented algorithm. The dosimeter had to be flexible in size, thin, high resolution, and easy to handle. Also it should be relatively energy-independent, tissue-equivalent both atomic number in physical density, two-dimensional, water resistant, and pose no risk of chemical exposure or suffocation to the patient during the irradiation time.[38,43] Among clinically available dosimeters such as ionization chambers, semiconductors, thermoluminescent dosimeters (TLDs), and radiographic films, radiochromic film was determined to be the most appropriate for this application.[38] It meets all the above requirements as well as being self-developing, relatively insensitive to light, and inexpensive.[38,39] The radiochromic film produces an image when radiation energy polymerizes the leuco dye within the film's sensitive layer, resulting in a color change proportional with dose.[38,43] The time lag between irradiation and film stabilization is short.[46]

However, a twenty-four hour waiting time (from irradiation to scanning) was selected for consistency and convenience within this study.

1.4 Goal of the Study:

The goal of this study is to characterize the differences between measured radiation dose and calculated radiation dose at the level of the air–hard palate interface for dogs undergoing nasal SRT. Measured dose is quantified utilizing Gafchromic EBT film. The Varian Eclipse Anisotropic Analytical Algorithm (AAA) will be utilized to determine the calculated dose as part of the SRT plan. Data collected from both a head phantom, constructed from a canine skull and soft tissue-equivalent substance (STES),[42] and dogs with spontaneously-occurring nasal tumors will be evaluated. Upon characterization of the differences between measured and calculated radiation dose, proper consideration can be given to patients with nasal tumors to avoid poor estimation of the dose delivered to oral mucosa in an effort to minimize the potential for complications.

CHAPTER TWO

MATERIALS AND METHODS

2.1 Canine Head Phantom

The canine head phantom was constructed from a canine skull and a soft tissue-equivalent substitute (STES). STES was selected because its density is equivalent to that of human soft tissue[42] (1.04 g/cm^3) and it provides an x-ray attenuation coefficient similar to soft-tissue based on International Commission on Radiation Units and Measurement ICRU-44. [44] STES was created by combining equal weights of urethane (PMC-121/30, part A, Smooth-On Inc, Easton, PA) and rubber (PMC-121/30 DRY, part B, Smooth-On Inc, Easton, PA) which were carefully mixed with 2.8 % powdered calcium carbonate by weight to ensure a homogenous mixture with minimal air bubbles or undissolved calcium carbonate. The mixture was left at room temperature for about 10-15 minutes to thicken and ease further handling. STES was poured into the foramen magnum filling the interior of the skull to represent the brain. A thin layer was poured to cover the hard palate and represents the oral mucosa. Subsequent layers were added to exterior of the canine skull to represent eyes, muscles, gingiva, connective tissue, and adipose tissue (Fig. 2.1).

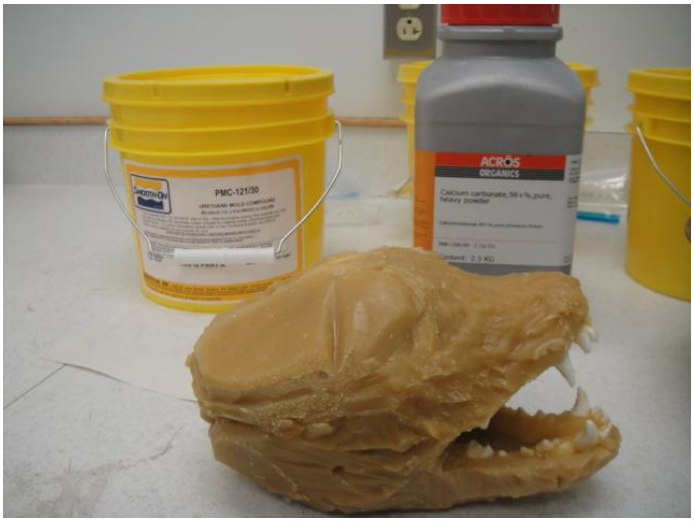

Figure 2.1 Canine head phantom constructed from canine skull and STES (rubber, urethane and calcium carbonate)

2.2 Radiochromic Film

Gafchromic®EBT film, by International Specialty products, Inc (ISP) in Wayne, NJ, from lot#: 48022-01I, was used for all measurements. Gafchromic®EBT film is a two-dimensional dosimeter[38,45] that was chosen for its unique properties[38,46] which fit the experimental design of this study. The film is composed of two active layers, each is 17 microns thick and separated by a 6 microns thick surface layer. The active layers are sandwiched between two, 97 microns thick, clear polyester sheets (fig 2.2.1).[43,49] The film has a near tissue-equivalent density and an effective atomic number (Z_{eff})= 6.98 (Z_{eff} of water=7.3), creating radiation absorption and scattering patterns equivalent to soft tissues.[39,45,46] Z_{eff} is a measure of electrostatic interaction between the nucleus and the surrounding electrons accounting for the screening effect by inner-shell electrons.[68] In a heterogeneous

compound like EBT film, Z_{eff} is calculated by a special formula that takes the fraction and atomic number of each component into consideration.[69] The atomic composition of Gafchromic®EBT film has been slightly modified compared to its predecessors Gafchromic®MD-55 and Gafchromic®HS (table 2.1).[39] The EBT film has a trace amount (0.3%) of Chlorine (Z=17) in its atomic composition, and the manufacturer claims that the presence of a moderate Z element in the EBT's atomic composition boosts the photoelectric absorption of KeV photons. Consequently EBT film exhibits a very low energy dependency, with a less than a 5 % difference difference between MeV and KeV ranges (fig2.2.2).[39] Several studies evaluated this claim,[45-48] a difference of less than 10 % was reported allowing for the use of EBT in the clinically applied range of energies.[45] The modified composition of the EBT sensitive layer resulted in a shift of absorption spectrum toward shorter wavelengths with peaks at 636 nm (fig2.2.3).[43] Upon scanning the film with an Epson Expression 10000 XL PHOTO model color scanner (Suwa, Nagano, Japan) that measures light transmission with three color bands: red, green, and the blue, using the red channel will maximize the sensitivity of the film since the film absorbs red light with more affinity than green or blue lights.[39] Devic *et al* 2009, suggests using the red channel for 0-4 Gy dose ranges, the green channel for 4-50 Gy and the blue channel greater than 50 Gy, to maximize precision and accuracy[51] (figure 2.2.4). However, two different reports indicate that the use of the red channel remains appropriate and well suited for radiation doses up to 8 Gy,[43,51] given that the sensitivity curve saturates around 10 Gy.[51]

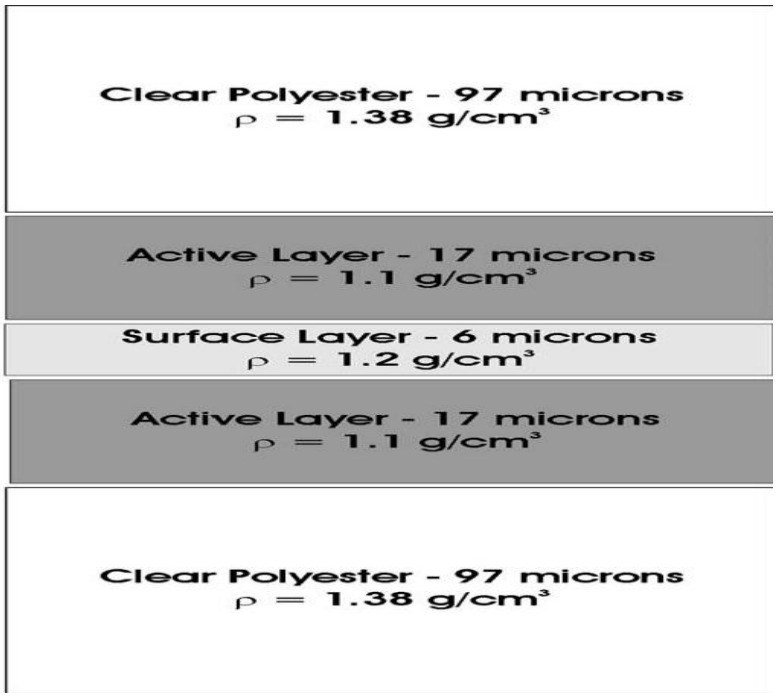

Figure 2.2.1 Gafchromic® EBT Film(43,49)

Table 2.1 Atomic composition and effective atomic number of GAFCHROMIC® EBT Dosimetry Film (39)

Atomic Composition						$Zeff = [\Sigma \alpha i (Zi)a]^{1/a}$
C	H	O	N	Li	Cl	
42.3%	39.7%	16.2%	1.1%	0.3%	0.3%	6.98

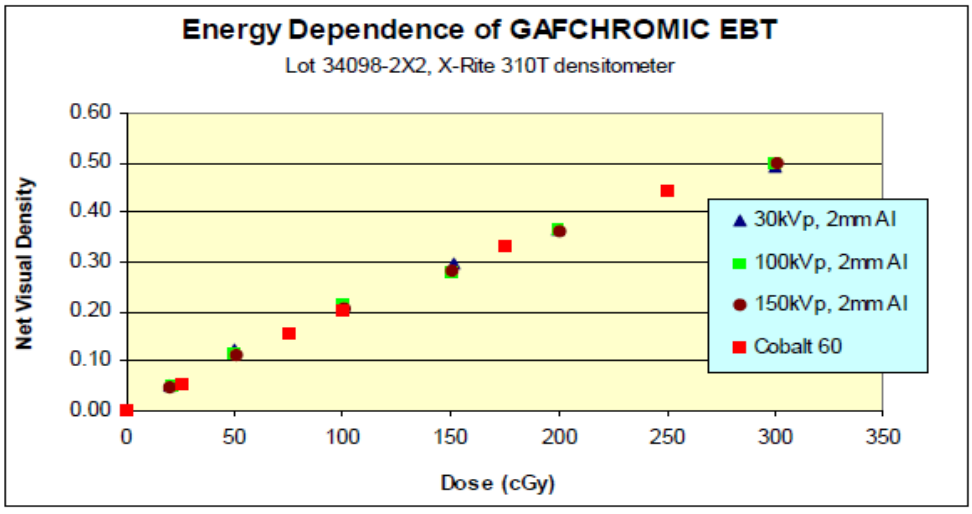

Figure 2.2.2 Energy dependence of GAFCHROMIC® EBT Dosimetry Film (39)

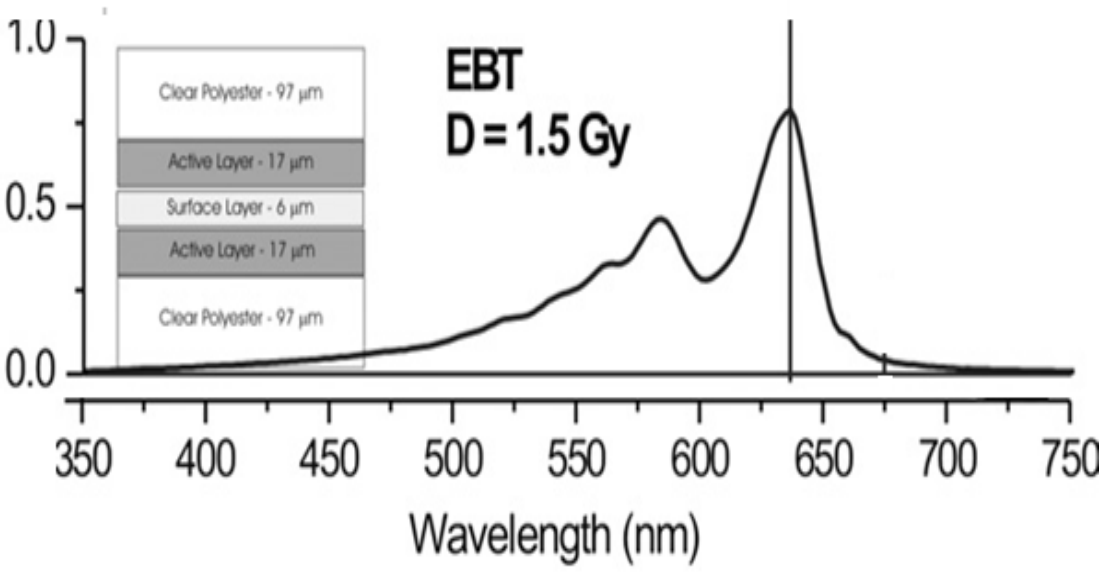

Figure 2.2.3 Absorption spectra for different GAFCHROMIC® EBT Dosimetry Film (43)

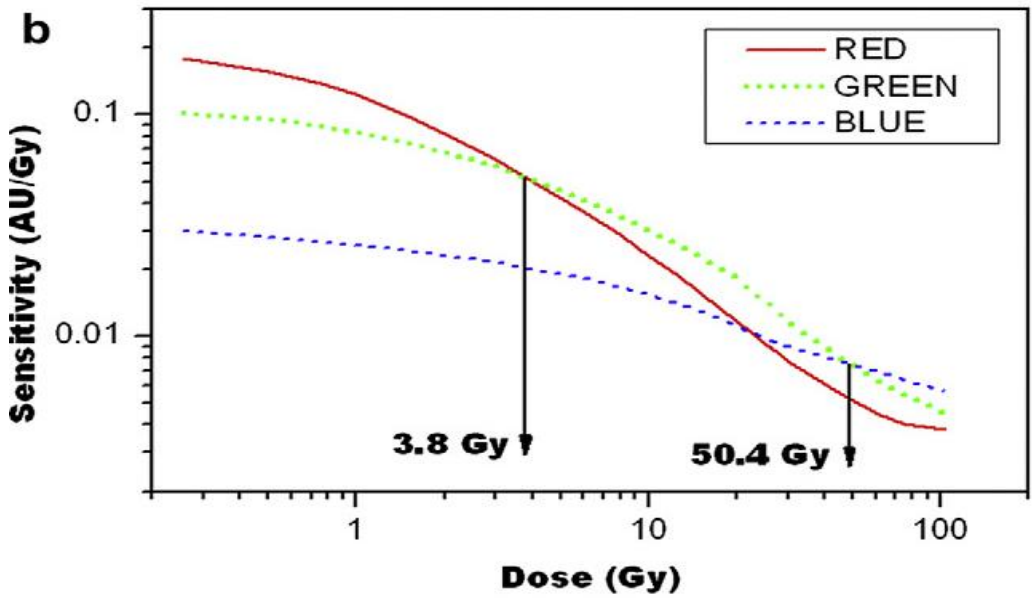

Figure 2.2.4 Sensitivity curves for the three color channels, arrows indicate the cross-over doses between the highest sensitivities for the three color channels (43)

Gafchromic®EBT film has a high resolution.[39] It is insensitive to light and does not require post-exposure chemical treatment (real-time development).[46] The image is formed through a polymerization process as the energetic particle deposits

its energy to the receptive part of the colorless monomer molecule.[38,43,51] The post-exposure density growth is a function of time. The manufacturer states an effective completion of development in less than two hours. A larger post-exposure growth is seen at lower doses than at higher doses. However most protocols suggest an interval of at least 8 hours between exposure and scanning to allow for stabilization of the film darkening.[43,52,56] Prior to exposure, the film was cut into a 1x3 cm elongated hexagon and fiducial markers were placed at the rostral and caudal most pointed ends. The caudal aspect of the film was marked for indexing purposes. Before and after exposure, the films were kept in a closed box inside the dark envelope provided by the manufacturer to avoid exposure to light.

2.3 Treatment Plans

2.3A Computed Tomography (CT) scans Acquisition and Contouring

A Philips Gemini TF big pore scanner within the CSU-ACC was used to acquire the initial planning CT images for both the phantom and client owned dogs. 2mm thick slices and a 512x512 image matrix were selected to achieve the desired image contrast and resolution. An individualized cranial immobilization device (Fig 2.3A), as previously described in Harmon et al.[36] and used at CSU-ACC was created for the phantom and each dog at the time of the initial CT scanning, and utilized for subsequent treatments to minimize inter-fractional setup errors.[36,53] The non-invasive immobilization system is comprised of a baseplate, support bridge, thermoplastic bite block, vacuum head and neck cushion and thermoplastic mask.[36]

The Varian Eclipse treatment planning software V8.6 and the Analytical Anisotropic Algorithm (AAA) version 8.6.15 utilize electron density information from imported planning CT scans together with scattered kernels modeled by Monte Carlo calculations to predict photon dose distributions.[26-28,49,57,58] A 2 mm calculation matrix was used for calculating the dose throughout the study. The gross tumor volume (GTV) was defined individually for each dog as the gross, identifiable disease on the planning CT.[53] In the phantom, GTV was constructed to occupy part of the right nasal cavity. In all cases, a 2 mm symmetrical expansion was applied to the GTV to create the planning treatment volume (PTV). This 2 mm accounts for the potential geometric (systematic) and residual (random) errors throughout the course of treatment and ensures prescribed dose to be delivered to PTV at least 95% of the time when OBI kV imaging is not used.[36] Adjacent normal structures (eyes, brain, skin) were contoured. To maximize radiation dose to the target (99% to the GTV and 95% to the PTV) while minimizing the dose to normal surrounding structures, a specification of dose-volume constraints and/or dose limits is made by the clinician, the software will try to get the most suitable configuration and weight of the radiation beams to achieve the intended dose prescription, in a process called inverse planning.[32]

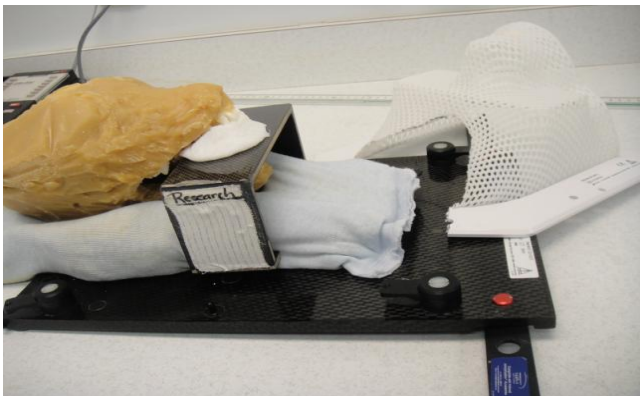

Fig 2.3A Cranial immobilization system used for the phantom composed of (mask, bite block, bridge, cushion, and baseplate)

2.3B Fields Selection and Dose Prescription

2.3B. 1 Phantom Plans

For the phantom, five identical SRT plans were created and subsequently delivered. In each plan a total dose of 30 Gy was delivered in three equal fractions (10 Gy/fraction). The GTV measured 22.4 cm^3 while the PTV had a volume of 34 cm^3. Seven isocentrically placed fields with gantry angles of (0, 51, 102, 153, 204, 255, and 306) degrees were constructed to deliver the dose (Fig 2.3B). Maximum doses to targets and sparing normal surroundings are achieved by the inverse planning technique as well as the use of dynamic multileaf collimator (dMLC), which modulates the intensity of delivered dose by the movement of the leaves across the aperture.[32]

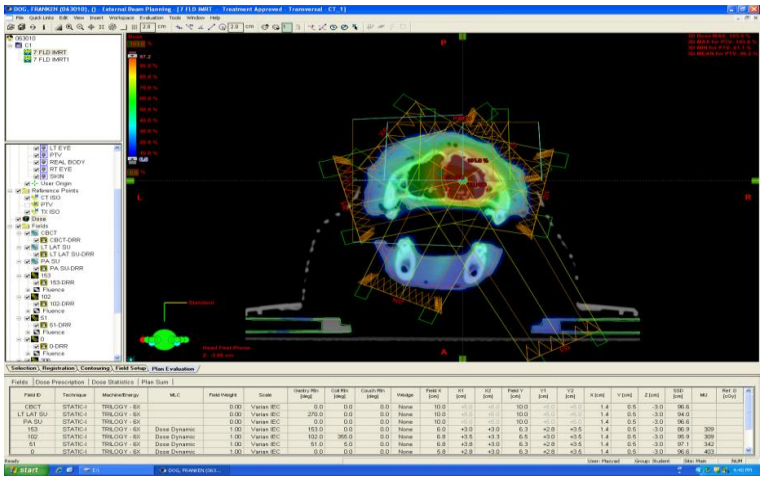

Fig 2.3B Phantom treatment plan showing PTV, fields, and dose distribution

The same treatment plan for the phantom was copied and normalized to establish four separate plans each with the same relative distribution of dose, but delivering escalating total doses of 2, 4, 6, and 8 Gy in a single fraction. These plans were normalized to deliver 99% of the planned dose to PTV. Within the PTV, a region of dose distribution consistent with the prescription and along the mucosa of the hard plate was identified for film placement. The aim of these four plans was to check for the film sensitivity in measuring escalating doses.

2.3B. 2 Dogs with Spontaneously-Occurring Tumors' Plans

Dogs, suffering from nasal tumors confirmed by tissue biopsy and/or suggested by head and neck CT that were treated with SRT, were selected to participate in this study. Procedures similar to that used for the phantom planning were conducted for individualized dogs. A high variation in size, extent, and location of the GTV was found across dogs. The CSU standard-of-care SRT approach was used to treat all client owned dogs from which data were obtained secondary to

the treatment. The dose prescription for the 13 dogs included in the study was 30 Gy given in three once daily fractions for three consecutive days. The median volume of the PTV in these dogs was 81.8 cm^3 with a range of 24.5- 273.3 cm^3. 100% of the dose was planned for 95% of PTV volume, and the median dose to 95% of PTV was 27.5 Gy. Median of seven fields, range (6-12), were constructed to deliver the dose.

2.4 Plan Delivery

Prior to irradiation, a region of relatively high surface dose (fig 2.4.1) was identified for all plans, phantom and client owned dogs. A prepared piece of film was placed in this region and was secured with 0.15 mm thick 3M transpore tape (St Paul, MN). For the phantom, the roof of the oral cavity was marked to identify the margins of the film to ensure consistency between treatment fractions and subsequent measurements (fig 2.4.2). Client owned dogs were under general anesthesia throughout each treatment session to avoid motion. The individualized immobilization system, created at the time of the planning CT, was applied during each treatment session to ensure adequate targeting of the tumor volume, while minimizing the impact of errors in daily setup.[36,53] The table shifts, as calculated by Varian Eclipse planning system, were applied to bring the isocenter of the beams into alignment with the isocenter of the tumor (fig 2.4.3). The On-Board Imager (OBI) uses kilovoltage X-rays (kV) to produce a high contrast image. An orthogonal pair of kV x-rays were captured prior to each treatment, and subsequently compared to digitally reconstructed radiographs (DRRs) from the planning CT.

Matching kV and DRR images ensures exact positioning of the patient based on bony structures is also known as image guided radiation therapy; (IGRT) (fig 2.4.4).[54,36] The orthogonal OBI kV delivers a dose to the patient of 1-3 mGy of air kerma per image, which is considered small when compared to the radiation treatment dose and was neglected in further analyses.[67] Table shifts were immediately applied based on the matching of the DRR and kV images. Radiation treatment was delivered by the Varian Trilogy linear accelerator with 6 MV photons at 100 cm source-to-axis distance (SAD).

After treatment, OBI was used again to acquire a cone beam CT (CBCT). CBCT allows for the subsequent soft tissue match needed to determine calculated dose to the mucosa of the hard plate.[54] CBCT was acquired as a high quality head image in 2 mm thick slices using a 512 x 512 matrix. The CBCT was registered (fused) with the planning CT and the fiducials on the EBT film strip were used to locate the position of the film on the hard palate at the time of treatment. The OBI CBCT delivers around 72-74 mGy CTDI (computed tomography dose index) to the patient per acquisition which is considered low as compared to treatment dose.[67] The contributing dose from CBCT was ignored in further analyses. Following exposure, the film was protected from light exposure and scanned 24 hours later.

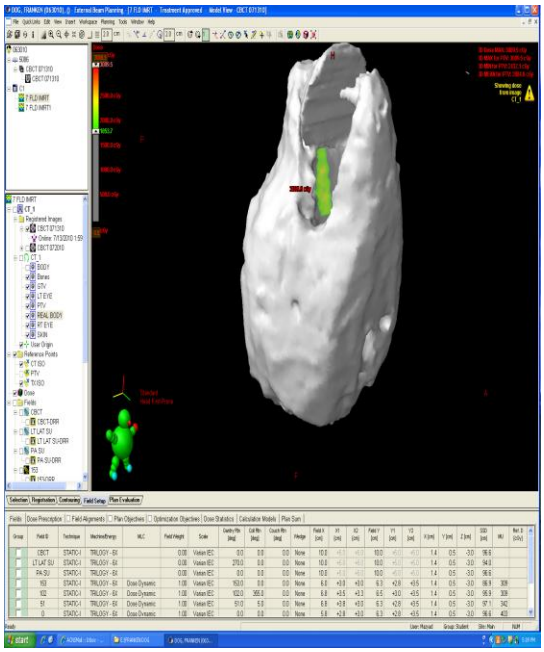

Figure 2.4.1 Identifying the surface dose using Varian Eclipse planning system

Figure 2.4.2 Film edges as identified on phantom

Figure 2.4.3 Laser beams used to identify treatment isocenters

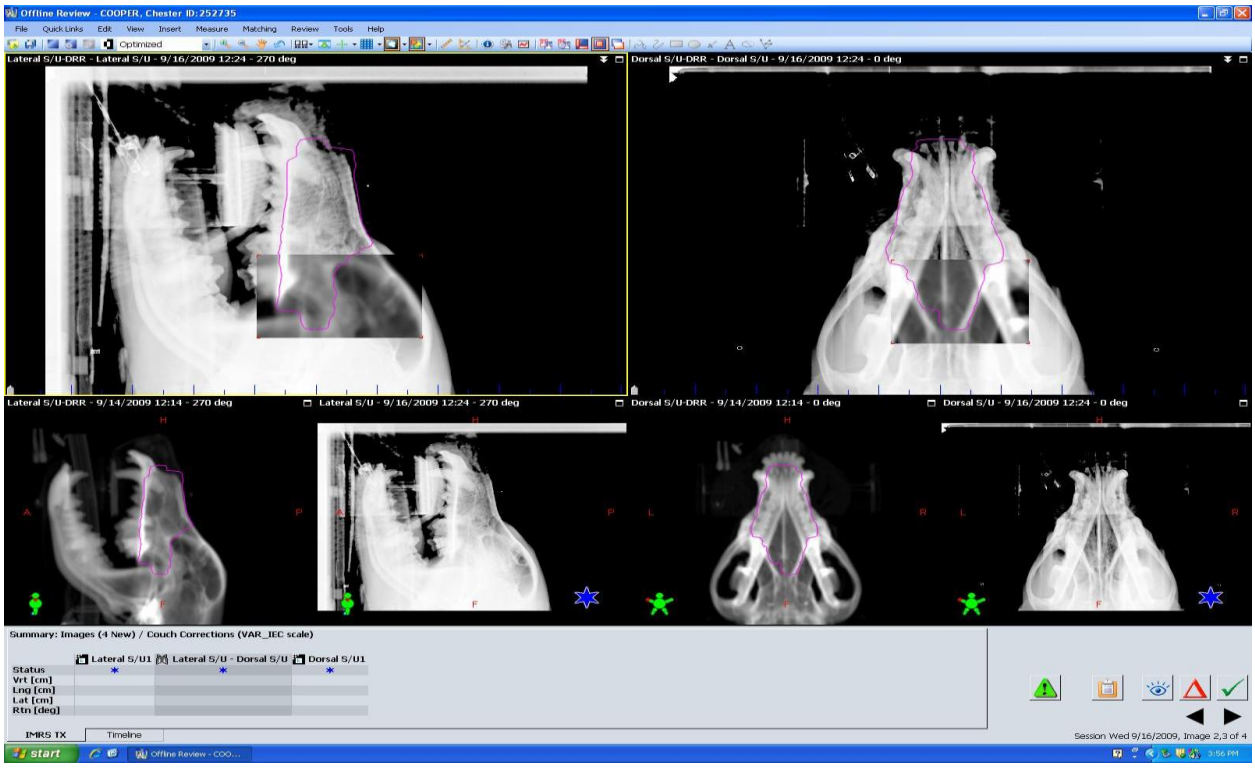

Figure 2.4.4 OBI-kV used to verify accurate alignment-prior to treatment

2.5 Calibration of Film Analysis System

Radiation energy polymerizes the dye in the active layer of Gafchromic®EBT film to produce darkening (blue in color) with intensity proportional to the dose of radiation.[38] To convert the darkening to radiation dose, a calibration curve must be created. Accompanying each treatment delivery, a blank sheet of film (8"x 10") was irradiated with 1000 monitor units (MUs) at a source-to-surface distance (SSD) of 95 cm via 13 steps resulting in a step wedge (Fig 2.5). Dose points in Table 2.2 were chosen to give film optical density (OD) values above and below the planned range of dose exposures. To best model dose distribution and back scatter while irradiating film with a step-wedge plan, the films were placed between 5 cm of

plastic water™ above and 10 below the film. Plastic water™ by Fluke Biomedical has megavoltage radiological properties similar to water within 0.5%.[50] The MLC is used to create 13 steps, where the maximum dose is delivered to the first step and the minimum dose is delivered to the last step. The above process was repeated multiple times to compare calibration curves and to determine any uncertainty in film/film analysis software responses, and precision. An ion chamber was used to verify the dose of the step-wedge plan. The measured charge (nC) was converted into actual dose by applying a cGy/nC conversion factor for the specific geometry. These measured doses were compared to those calculated by the Varian Eclipse software for further verification.

Figure 2.5 Gafchromic EBT film post step-wedge plan exposure

Position (cm)	Measured Dose for 1000 MUs
Rel to ISO	cGy
-12	104.5
-10	183.2
-8	260.7
-6	338.2
-4	415.6
-2	490.4
0	567.8
2	645.3
4	725.5
6	800.7
8	874.3
10	942.7
12	989.5

Table 2.2 Step –wedge dose values relative to position

2.6 Post-Exposure Scanning and Measurement using the Flatbed (Epson) Color Scanner and QA Film Analysis Software

Following each exposure, the film was cured for 24 hours, then three films: patient (DATA) film, the step-wedge (SW) film, and the background (BKG) film, were scanned. All films were scanned using a commercial Epson Expression 1000 XL photo scanner.[39,52,55] Film orientation within the scanner was consistent for all films, the polarization axis of each piece of film was verified with the use of a polarized lense.[39] A ten minutes period was allowed for the scanner light to heat up and stabilize minimizing the potential for fluctuation. The film was placed near the center of the scanning area.[56] The film was scanned in the professional mode as positive film with 50 dpi resolution and no color correction. Scanning produced images that were saved as 48-bit "TIFF" format with no compression. These images are available in three channels: red, green, and blue.

After scanning, films were imported into FilmQA software version 2.2.0113 (3cognition LLC, Great Neck, NY). The red channel was used to import most of these films because of higher sensitivity within the expected dose range.[43,51] The step-wedge (SW) film and known dose values for each step were used to create a 5^{th} order polynomial calibration curve. Consistent size and shape region of interests (ROI) were drawn at the center of each step. Upon subtracting the background value measured by scanning an unexposed piece of film (BKG film), the corrected ROI pixel values with corresponding doses were used to create a calibration curve. Subsequently the DATA film was evaluated to determine dose at points specified

previously on Eclipse. An average of three measurements was calculated for each data point in order to reduce the statistical error. For phantom exposures, three points were identified on each DATA film (1, 1.5, and 2 cm as measured from the caudal end of the film). For DATA films from the treatment of client owned dogs, the points were limited to regions of adequate contact between the film and the roof of oral mucosa due to the presence of rugae.[25]

2.7 Post-Exposure Calculations

The Varian Eclipse treatment planning software uses an AAA algorithm to predict volume dose distribution.[57,58] After each exposure, a CBCT was acquired and fused with the original planning CT to identify the film position.[54] One or more reference points were selected within the treatment plan based upon contact between hard palate mucosa and the radiochromic film as determined by the fused CBCT and original planning CT. Calculated doses were compared to measured doses for the same reference points. Due to the potential for inter-fractional setup error of up to 2 mm,[36] a 2 mm radius sphere was created from each reference point. Minimum, maximum, and average doses across each sphere were recorded in addition to the reference point dose for further comparison and analysis.

CHAPTER THREE

DATA AND ANALYSIS

3.1 Dogs with Spontaneously-Occurring Tumors (General Information)

Table 3.1 lists the biological information for the 13 dogs with spontaneously-occurring nasal tumors included in this study. The median age of dogs at the time of presentation was 10 years, with a range of 5 to 12 years. Eight of the thirteen dogs were male (61.54 %), while the remaining five dogs were female (38.46 %). The male to female ratio was 1.6:1 (8/5). Several breeds were represented in this study. Mixed breed dogs were seen most frequently (30.77 %). Eleven of the thirteen dogs (84.6 %) had biopsy-confirmed nasal tumors of epithelial origin and only two dogs had a biopsy confirmed nasal tumor of mesenchymal origin (15.4 %). A majority of these tumors were located in one nasal cavity 84.6 % (11/13), the right nasal cavity in 69.2 % (9/13) of the dogs while left and both cavities were occupied in 15.4 % (2/13) each. Median volume of the PTV in these dogs was 81.8 cm^3 with a range of 24.5- 273.3 cm^3. Local invasion of the cribriform plate was identified in 30.77 % (4/13) of the dogs at the time of diagnosis.

Table 3.1 General information about dogs and their nasal tumors

Dog	Age	Sex	Breed	Type	Site	PTV volume (cm^3)
A	11	MC	Mix	Poorly differentiated adenocarcinoma	Right	63.4
B	10	M	Labrador Retriever	Nasal adenocarcinoma	Right	120.7
C	7	FS	Lhaso apso	Nasal adenocarcinoma	Right +Left+ Invasion	24.5
D	11	FS	Golden Retriever	Nasal adenocarcinoma	Right +Invasion	77.3
E	11	MC	Mix	Nasal chondrosarcoma	Right	59.4
F	10	FS	Mix	Nasal adenocarcinoma	Right + Left	154.7
G	13	FS	Sheltie	Transitional carcinoma	Right	81.8
H	11	M	Golden Retriever	Nasal adenocarcinoma	Right +Invasion	167
I	5	MC	Old English sheepdog	Nasal adenocarcinoma	Right	273.3
J	8	FS	Vizsla	Nasal carcinoma	Right	47.1
K	9	MC	Scottish terrier	Nasal carcinoma	Left	94.1
L	8	MC	Mix	Nasal sarcoma (probably Chondrosarcom)	Right	52.7
M	5	MC	German Shepherd	Nasal adenocarcinoma	Left +Invasion	91.9

M: male, MC: male castrated, FS: female spayed

Nine of the dogs were examined at least once following SRT for the development of radiation related adverse effects by retrospectively evaluating the CSU ACC medical records through June 2011. Adverse effects, reported during scheduled recheck examinations or when clients sought patient care, were retrospectively scored based upon documentation within the medical record. Effects were scored according to VRTOG acute and late radiation-induced side effects scoring scheme (Table 1.1). Five of the nine dogs (55.6 %) developed appreciable acute adverse effects. One dog (11.1 %) developed a grade II late effect in the form of a cataract, this dog had an ocular exam suggestive of cataract prior to treatment. One-third of the dogs experienced appreciable skin adverse effects. All of the skin effects seen were self-limiting grade I acute effects in the form of alopecia (3/3), skin erythema (1/3), and hyperpigmentation (1/3). Two dogs (22.2 %) developed acute effects within the mucous membranes of the oral cavity. There was one incident of grade I erythema of the oral cavity and one incident of grade II mucositis of the oral cavity. Two dogs developed ocular complications associated with radiation therapy, which were presented as two dogs with grade II keratoconjunctivitis sicca, one dog with grade II anterior uveitis, one dog with a grade III corneal ulcer, and one grade II cataract. Table 3.2 lists the adverse effects noted in the nine dogs with at least one documented physical examination following completion of the nasal tumor SRT protocol at CSU-ACC.

Table 3.2 Adverse effects and times of development in client owned dogs following nasal SRT treatment at CSU-ACC

Dog	Follow up exams after SRT (weeks)	Oral Mucosa adverse effects	Grade	Acute/ Chronic	Skin adverse effects	Grade	Acute/ Chronic	Eye adverse effects	Grade	Acute/ Chronic
A	2 32	None			None			None		
B	1	None			None			None		
C	8 12 14 26 27	None			Alopecia (8 weeks)	I	Acute	KCS Corneal ulcer (14 weeks)	II III	Acute Acute
D	12	Erythema (12 weeks)	I	acute	Focal area of hyperpigmentation Alopecia (12 weeks)	I I	Acute Acute	None		
F	4 6	Mucositis (4 weeks)	II	acute	None			None		
G	4	None			None			Catarct KCS Ant. Uveitis (4 weeks)	II II II	chronic Acute Acute
I	2 4	None			Alopecia Skin erythema (2 weeks)	I I	Acute Acute			
K	1				None			None		
M	2 3 8	Ulcer before Rx that didn't progress after RX			None			None		

3.2 Film System Commissioning

3.2A Dose Verification for the Step-Wedge Plan

An ion chamber (PTW, N30013-1812) was used to measure charge (nC) of each step in SW film. A cGy/nC conversion factor was applied to convert measured charge into actual dose (cGy). These measured doses were compared to those calculated by the Varian Eclipse software for further verification. The median percent difference between measured and calculated dose, for 500 MUs plan, was 0.4%, with a range of -0.2 to 0.9. The minimal difference of 0.0 % was seen at a calculated dose of 400.3 cGy and the largest difference of 0.9% was seen at a calculated dose of 90.8 cGy. To deliver 1000 MUs, the 500 MUs plan was delivered twice and doses were scaled from doses measured at 500 MUs (Table 3.3).

Table 3.3 Step-wedge film readings by Ion chamber and Eclipse

Position (cm)	Measured Charge	Measured Dose for 500 MUs	Eclipse Dose for 500 MUs	Measured Vs Eclipse Difference	Measured Dose Scaled to 1000 MUs
Rel to ISO	*nC*	*cGy*	*cGy*	*%*	*cGy*
-12	**8.151**	**52.3**	**52.1**	**0.4**	**104.5**
-10	**14.287**	**91.6**	**90.8**	**0.9**	**183.2**
-8	**20.330**	**130.3**	**129.6**	**0.5**	**260.7**
-6	**26.380**	**169.1**	**168.1**	**0.6**	**338.2**
-4	**32.410**	**207.8**	**207.0**	**0.4**	**415.6**
-2	**38.250**	**245.2**	**245.8**	**-0.2**	**490.4**
0	**44.280**	**283.9**	**284.4**	**-0.2**	**567.8**
2	**50.330**	**322.7**	**323.1**	**-0.1**	**645.3**
4	**56.580**	**362.7**	**361.4**	**0.4**	**725.5**
6	**62.450**	**400.4**	**400.3**	**0**	**800.7**
8	**68.190**	**437.2**	**435.6**	**0.4**	**874.3**
10	**73.520**	**471.3**	**469.2**	**0.5**	**942.7**
12	**77.170**	**494.7**	**492.3**	**0.5**	**989.5**

3.2B Precision Validation of EBT Film and Film Analysis Software

To validate the precision of Gafchromic EBT film and Film QA software used for analysis, calibration curves, created from 6 different SW films exposed on separate days, were compared (Fig 3.2B). The coefficient of variation (CV) for each applied dose in the step-wedge plan was calculated from the mean and standard deviation (STD) of the six corrected pixel values corresponding with each step. The variations in the corrected pixel value among the different response curves were minimal as seen in Table 3.4.

Table 3.4 Variation in each dose step comparing six calibration curves

Applied dose (cGy)	Mean (PV)	STD (PV)	CV%
989.5	13375.1	329.0526	2.460187
942.5	13781.46	338.2287	2.45423
874.3	14471.73	294.8532	2.037443
800.7	15246	294.2739	1.930171
725.5	16155.59	307.1336	1.901098
645.3	17241.42	288.4773	1.673165
567.8	18528.97	310.8582	1.677688
490.4	20100.35	309.707	1.540804
415.6	22078.33	327.286	1.482386
338.2	24517.55	303.5884	1.238249
260.7	27815.25	282.6276	1.016089
183.2	32489.28	262.9642	0.809387
104.5	39532.64	415.1527	1.050152
0	57042.27	396.9905	0.695959

PV: Pixel Value

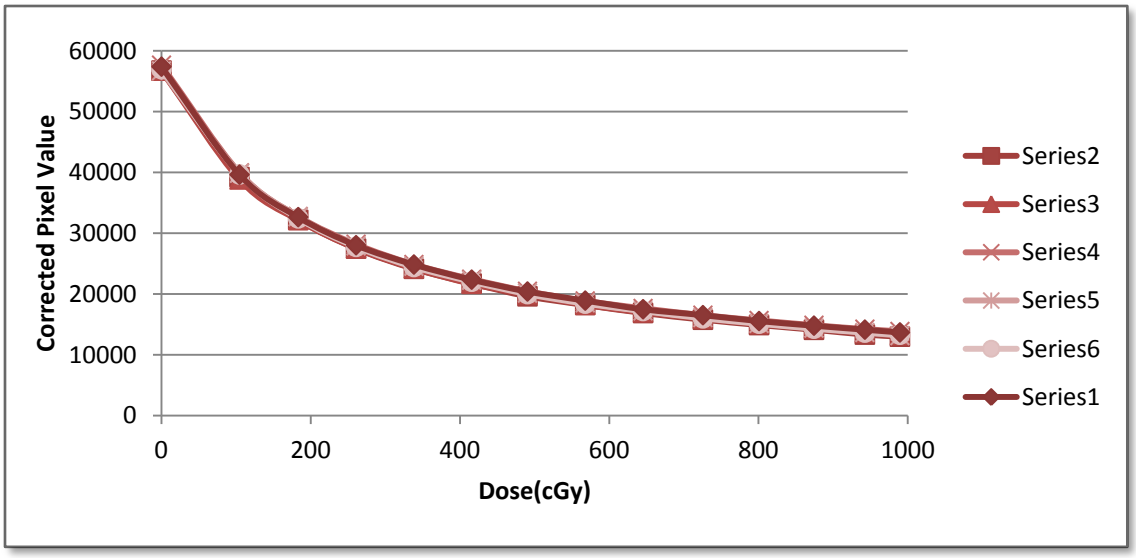

Figure 3.2B Comparison of six different calibration curves created from corresponding Step-wedge film by FilmQA software

3.2C Dose Escalation Validation of EBT film and Film Analysis Software

Four plans were copied from the original plan to treat the phantom. Each plan was normalized to achieve the desired dose with the same relative dose distribution at the level of the DATA film placement along the mucosa of the hard palate. Single fraction doses of 2, 4, 6, and 8 Gy were delivered. Three points 1, 1.5, and 2 cm respectively from the caudal margin of the film were selected as reference points to evaluate and compare both measured and calculated dose. An average of the three points' measured values was recorded for each plan. By plotting the relationship of the calculated and measured dose with the corresponding plan (figure 3.2C), an obvious linear relationship was demonstrated for each of the four different plans, with slope of around 89 cGy and intercept of 11 cGy. A fourth order polynomial curve best represented the relationship between the measured and calculated doses.

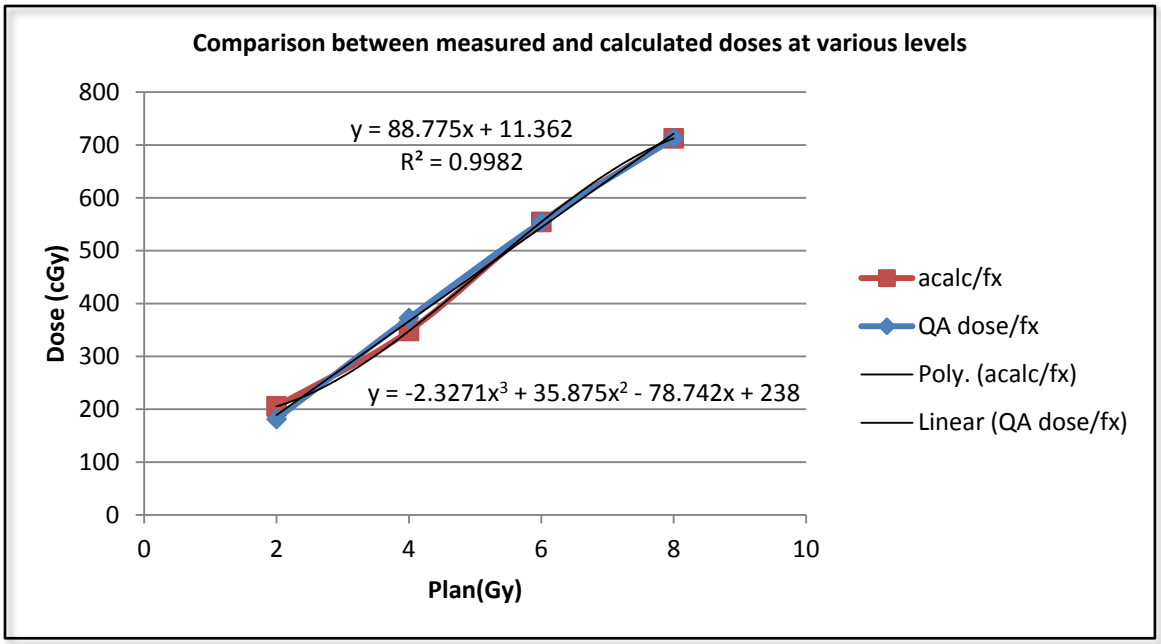

Figure 3.2C Dose escalation plans with correspondent measured and calculated values

3.3 Phantom Data Analysis

3.3A Point-to-Point Comparison

Three reference points were identified at locations of (1, 0.5), (1.5, 0.5), and (2, 0.5) from caudal margin of each DATA film (3x1 cm). The doses at each reference point were first calculated via Eclipse (pcalc) then measured via EBT film and FilmQA analysis system. The failure to meet assumption of normality and homoscedasticity of data distribution allowed for the use of a Spearman rank correlation test to prove covariance between the two groups of points. There was no evidence of significant correlation between measured and calculated doses given $r = 0.016$ with a p-value = 0.9.

After evaluating the distribution of differences for normality, a paired t-test was used to compare measured and calculated dose. This method of data analysis revealed that dose as calculated by Varian Eclipse underestimates the measured dose delivered to oral mucosa by a mean dose of 112.7 ± 109.5 cGy (p-value of <0.0001) (table 3.5).

Table 3.5 Phantom Data: Comparison of measured point dose- to-calculated point dose

Variable	N	Mean	95% Confidence Limits	STD
Measured Doses	**45**	**565.05 cGy**	**558.7- 571.4 cGy**	**21 cGy**
Calculated Doses at Reference Points	**45**	**452.4 cGy**	**420.5-484.3 cGy**	**106.2 cGy**
Differences (Measured-Calculated)	**45**	**112.7 cGy**	**79.8-145.6 cGy**	**109.5 cGy**
Percent Difference [(Measured-Calculated)/Calculated]	**45**	**32.7 %**	**21.9-43.5 %**	**35.1 %**

N sample size

3.3B Point-to-Average Comparison

Due to the high variation in calculations at reference points, and in an effort to overcome the potential 2 mm inter-fractional positioning uncertainty, 2 mm radius spheres were created with the reference point at the center of the sphere. Subsequently, measured doses at these points were compared to the average doses across spheres (acalc). Again, the Spearman rank correlation test was used due to the violation of the assumptions of correlation, which resulted in r equal to -0.06 and p-value of 0.7. The use of a paired t-test, in an effort to prove that the difference between measured and average calculated dose is equal to zero, revealed a mean difference of 103.7±102.7 (p-value <0.0001) (table 3.6).

Table 3.6 Phantom Data: Comparison of measured point dose-to-calculated average

Variable	N	Mean (cGy)	95% Confidence Limits (cGy)	STD (cGy)
Measured Doses	45	565.05	558.7 - 571.4	21
Calculated Average Doses	45	461.33	431.9 - 490.8	97.94
Differences (Measured- Calculated)	45	103.7	72.86 - 134.6	102.7

3.3C Point-to-Range Comparison

Since comparing measured dose to the average of calculated doses across each sphere did not solve the issue of high variance among calculations, point dose was tested against range (from minimum to maximum) of doses that represent the extremes of dose distribution in corresponding sphere (Fig 3.3C.2). All measured doses were found to be within the range of calculated doses. Each dose range was divided into 10 equal portions, frequencies of measured doses and calculated doses at reference points (pcalc) within each range were reported in table 3.7 (Fig 3.3C.1). Measured doses were located within a portion of the total dose range (0.4-0.8). A majority of the measured dose points were between the midpoint and 0.7 of the range (89%) and only few points were above or below this range. The distribution of calculated doses was spread over a wider range (0.1-0.8), and its peak was subtle and shifted more to the left when compared to measured doses. Further analysis on the build-up regions was performed (Table 3.8), revealing that, in the terms of doses, the majority of measured doses lie between 470.5 (95% confidence interval of median of midpoints' lower limit) and 659.5 cGy (95% confidence interval of median of 0.7 divisions' upper limit), while the median of calculated doses at the reference points (pcalc), which is equal to 450.7 cGy, is smaller than the above

interval's lower limit. However, both intervals overlap for a small region at the upper tail of pcalc.

Table 3.7 Frequency distribution of measured (QA) and calculated point (pcalc) within the normalized ranges of the spheres created around phantom reference points

Ranges	Percent(QA)	Percent(pcalc)
Below	0%	0%
0(Min)-0.1	0%	0%
0.1-0.2	0%	2%
0.2-0.3	0%	9%
0.3-0.4	0%	20%
0.4-0.5(Mid)	9%	33%
0.5(Mid)-0.6	47%	27%
0.6-0.7	42%	7%
0.7-0.8	2%	2%
0.8-0.9	0%	0%
0.9-1(Max)	0%	0%
Above	0%	0%
Total	100%	100%

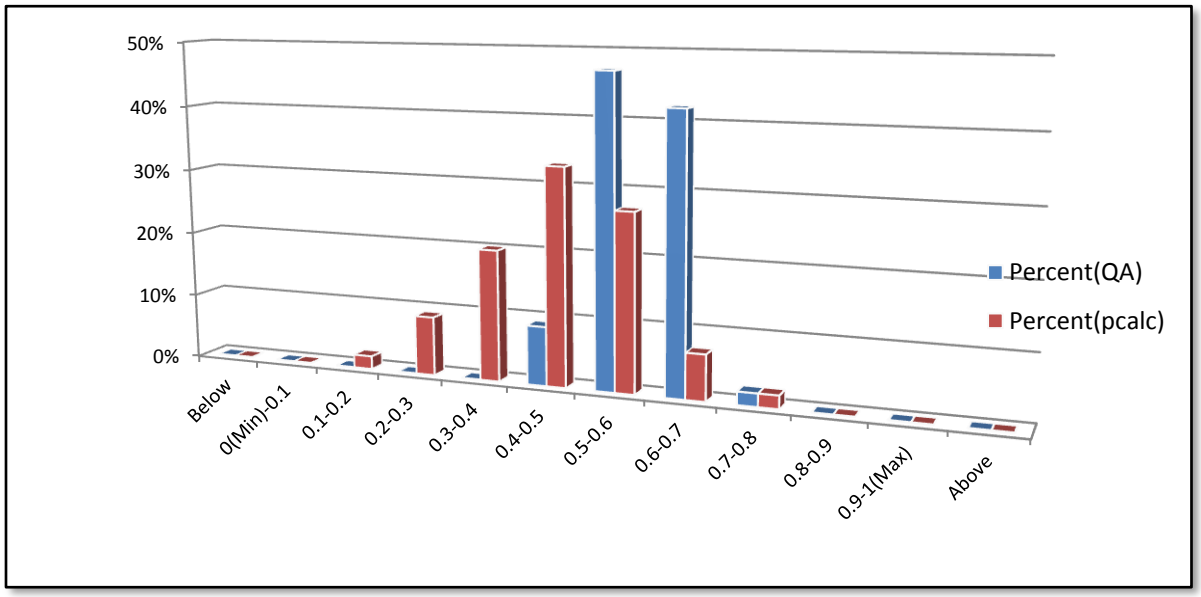

Figure 3.3C.1 Measured (QA) and calculated (pcalc) doses in relationship to the ranges of calculated doses of phantom in percents

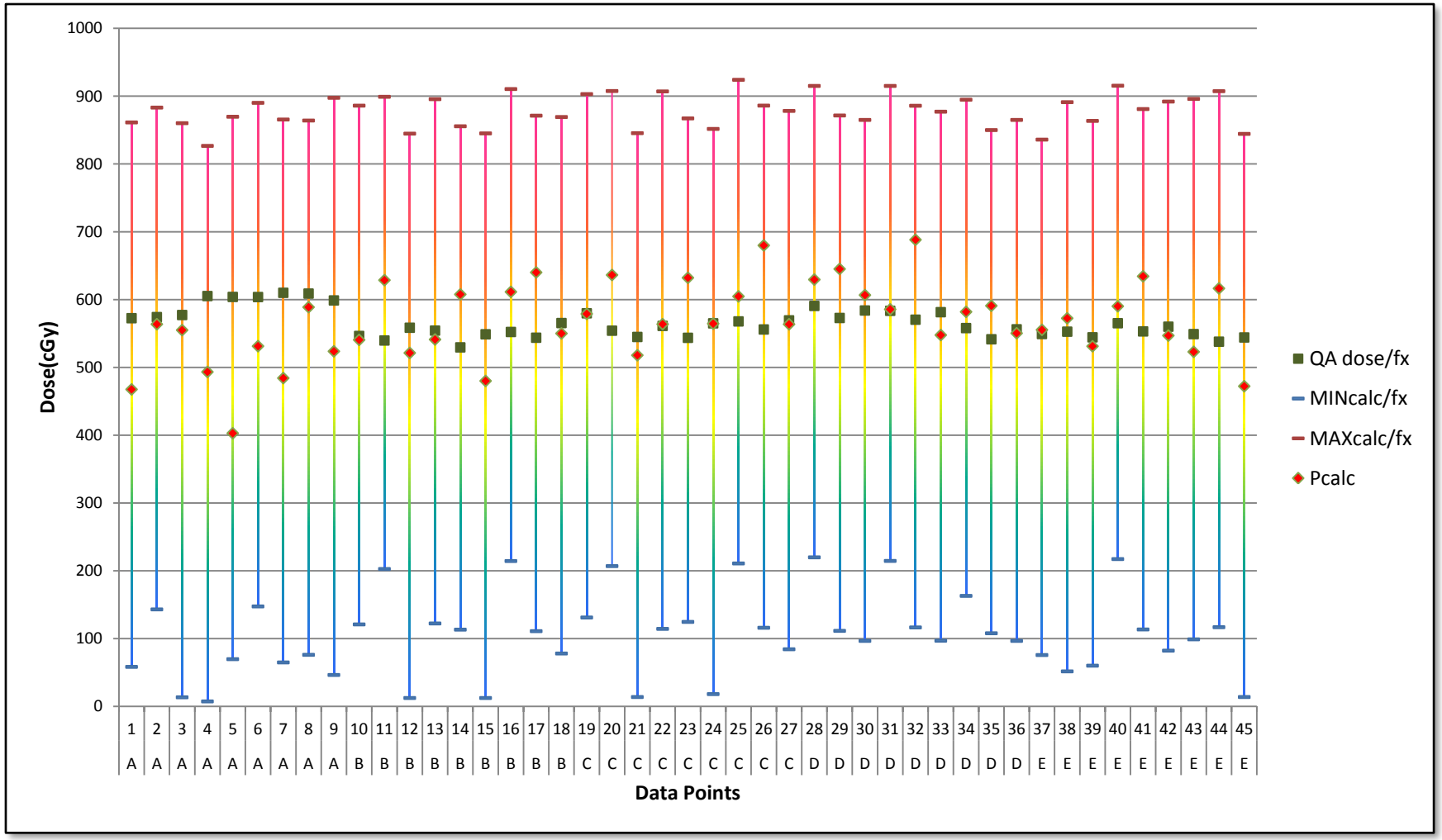

Figure 3.3C.2 Positions of measured doses (QA dose) and calculated doses at reference points (Pcalc) with respect to ranges of calculated doses across volumes created in phantom plans

Table 3.8 Median and 95% confidence limits of the ranges, regions in ranges, QA doses, and claculated doses at reference points of phantom

Variables	Median (cGy)	95% Confidence Limits (cGy)
Ranges	774.2	771.7 - 788.9
0(Min)	98.9	76 - 116.8
0.1	176.7	154.9 - 194.3
0.2	254.5	233.8 - 271.8
0.3	332.3	312.7 - 349.4
0.4	410.2	391.6 - 426.9
0.5(Mid)	488	470.5 - 504.4
0.6	565.8	549.4 - 581.9
0.7	643.6	628.3 - 659.5
0.8	721.5	707.2 – 737
0.9	799.3	786.1 - 814.5
1(Max)	877.1	865 – 892
Measured Doses (QA)	558.4	552.6 - 572.8
Calculated Doses at Reference Points (pcalc)	450.7	387.1 – 506

3.3D Range-to-Range Comparison

The high variability within calculated doses demonstrated the need to characterize the amount of variation Eclipse shows in predicting doses at air-tissue interfaces. So a new approach was adopted to analyze the existing data, where the minimum and maximum doses were selected for each phantom exposure to compare ranges created from minimum and maximum measured doses to those of average calculated doses (acalc) (Fig 3.3D).

If variation in dose prediction is close to that of measured dose, the median of the above ranges would be equal 1. Table 3.9 lists the results of comparing the range of measured doses to the range of calculated doses. Variations among the

FilmQA measured doses are much smaller than the variations among the Eclipse calculated doses with p-value of <0.0001. The ratio of minimum measured values to minimum calculated values was greater than one, while the ratio of maximum values was less than one.

Table 3.9 Phantom Data: Median values and 95% confidence limits of the ratios of ranges, minimums, and maximums values of measured and acalc doses.

	Median	95% Confidence Limits	p-value*
Range measured/Range acalc	**0.16**	**0.08 - 0.3**	**<0.0001**
Min measured/ Min acalc	**1.126**	**0.98 - 1.3**	**0.0026**
Max measured/ Max acalc	**0.936**	**0.9 - 1.04**	**0.0302**
Range measured (cGy)	**13.4**	**11.2 - 21.4**	
Range acalc (cGy)	**95.17**	**55 - 140.5**	

All reported p-values are by the use of signed rank test because data distribution is not normal

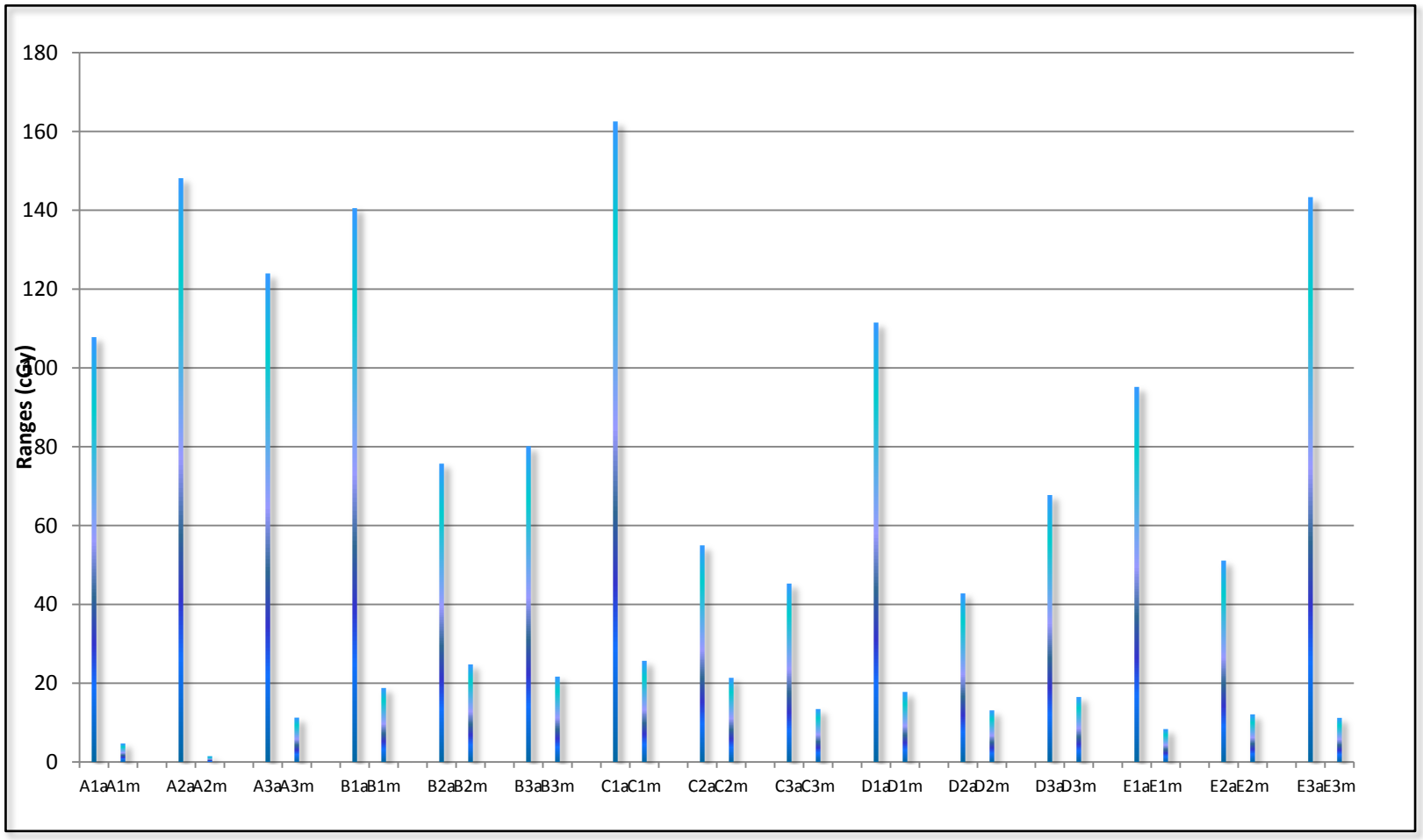

a: average calculated dose *m: measured dose for each phantom exposure*

Figure 3.3D Range of measured doses compared to range of average calculated doses in each phantom exposure

3.4 Dogs Data Analysis

3.4A Point-to-Point Comparison

The same analysis approaches applied to the phantom data were applied to the data collected from dogs undergoing SRT for their nasal tumors. Reference points were selected in each exposed DATA film anywhere there was appreciable contact between the film and the oral mucosa along the hard palate. The Spearman rank correlation test resulted in an r value of 0.44 and a p-value of 0.0024. A paired t-test comparing the differences between measured (meas) and calculated doses at reference points (pcalc) resulted in a mean of 64.4 ± 119.2 cGy. However, the results of the paired t-test could not be considered because the distribution of differences was not normal. A Wilcoxon two-sample exact test was used instead with a p-value of 9.2×10^{-5} (Table 3.10).

Table 3.10 Client Owned Dogs Data: Comparison of measured point dose- to-calculated point dose

Variable	N	Mean	95% Confidence Limits	STD
Measured Doses	**46**	**478.97 cGy**	**465.5 - 492.5 cGy**	**45.53 cGy**
Calculated Doses at Reference Points	**46**	**414.6 cGy**	**376.1 - 453.1 cGy**	**129.67 cGy**
Differences (Measured- Calculated)	**46**	**64.4 cGy**	**28.98 - 99.8 cGy**	**119.2 cGy**
Percent Difference [(Measured-Calculated)/Calculated]	**46**	**26.35 %**	**13.96- 38.7 %**	**41.7 %**

3.4B Point-to-Average Comparison

As performed previously with the phantom data, dose volumes as spheres were created based on 2 mm symmetrical expansions from the previously identified

reference points. The Spearman rank correlation found covariance between measured and averaged calculated (acalc) doses as proved by r=0.45 and p-value of 0.0016. Again the paired t-test reported a mean of 74±111.2 cGy with a p-value calculated by the use of Wilcoxon two-sample exact test of $4.2x10^{-5}$ (Table 3.11).

Table 3.11 Client Owned Dogs Data: Comparison of measured point dose- to-calculated average dose

Variable	N	Mean (cGy)	95% Confidence Limits (cGy)	STD (cGy)
Measured Doses	46	478.97	465.5 - 492.5	45.53
Calculated Average Doses	46	404.9	368.3 - 441.5	123.32
Differences (Measured- Calculated)	46	74	41.1 - 107.1	111.2

3.4C Point-to-Range Comparison

Measured doses were compared to the ranges that represent dose distribution in each sphere. Almost all doses measured by FilmQA were within the corresponding ranges with the exception of one point where the measured dose exceeded the maximum dose of the calculated range by about 3 % (Fig 3.4C.1). Table 3.12 shows that majority of the measured doses (90 %) are above the midpoint of the range, while very few are below (Fig 3.4C.2). The distribution of both measured and calculated doses appears wide, with measured appearing to have a slightly wider overall distribution. The peak of the calculated dose is higher and shifted more to the left when compared to that of measured doses. The medians of various components of the ranges were reported together with their 95 % confidence limits to correlate frequency distribution of data to intervals of doses (Table 3.13).

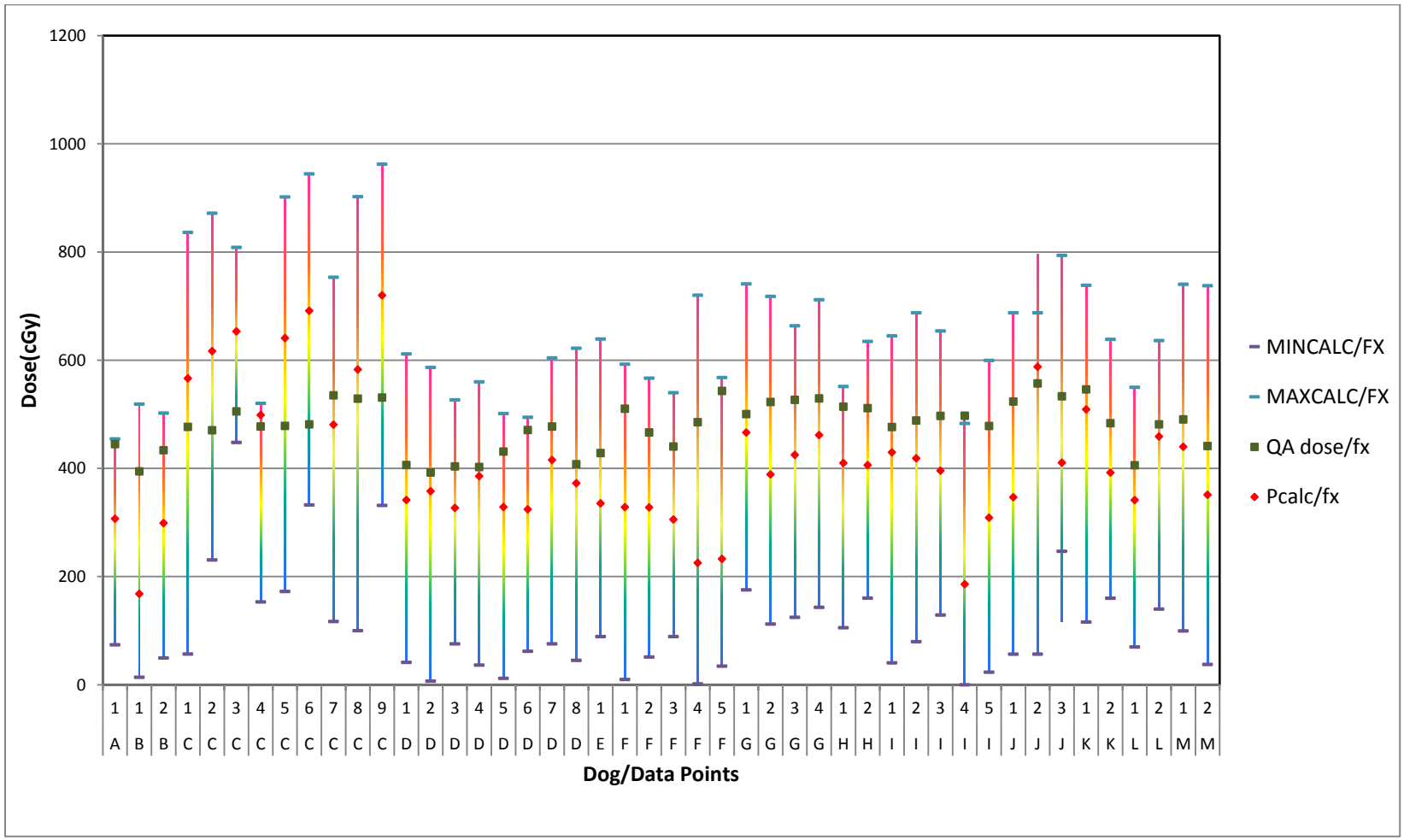

Figure 3.4C.1 Positions of measured doses (QA dose) and calculated doses at reference points (Pcalc) with respect to ranges of calculated doses across volumes created in client owned dogs' plans

Table 3.12 Frequency distribution of measured (QA) and calculated point (pcalc) within the normalized ranges of the spheres created around dogs reference points

Ranges	Percent(QA)	Percent(pcalc)
Below	0%	0%
0(Min)-0.1	0%	0%
0.1-0.2	2%	0%
0.2-0.3	2%	2%
0.3-0.4	4%	9%
0.4-0.5(Mid)	2%	15%
0.5(Mid)-0.6	11%	35%
0.6-0.7	30%	35%
0.7-0.8	26%	2%
0.8-0.9	11%	2%
0.9-1(Max)	9%	0%
Above	2%	0%
Total	100%	100%

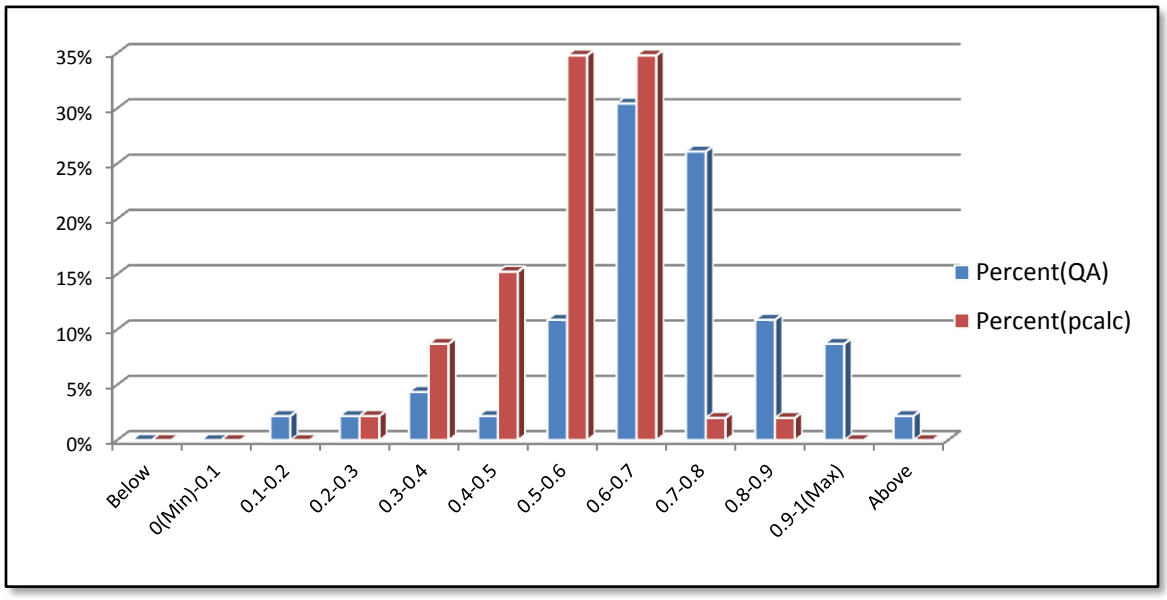

Figure 3.4C.2 Measured (QA) and calculated (pcalc) doses relation to the ranges of calculated doses of dogs in percents

Table 3.13 Median and 95% confidence limits of the ranges, regions in ranges, QA doses, and claculated doses at reference points of dogs

Variables	Median (cGy)	95% Confidence Limits (cGy)
Ranges	561.8	535.4 – 601
0(Min)	75.7	51.4 – 117
0.1	131.85	104.9 - 177.1
0.2	188	158.5 - 237.2
03	244.2	212 - 297.3
0.4	300.4	265.5 - 357.4
0.5(Mid)	356.6	319.1 - 417.5
0.6	412.8	372.6 - 477.6
0.7	468.9	426.2 - 537.7
0.8	525.1	479.7 - 597.8
0.9	581.3	533.3 - 675.9
1(Max)	637.5	586.8 – 718
Measured Doses (QA)	480	470.6 - 505.5
Calculated Doses at Reference Points (pcalc)	390.6	341.5 - 440.1

3.4 D Range-to-Range Comparison

To determine the degree of variation between the average calculated doses and the measured doses, the range from minimum and maximum measured doses for each dog were compared to the range of the minimum and maximum average calculated dose for the same dog (Fig 3.4D.1). Table 3.14 lists the results of this comparison. As demonstrated in the table, the variation among calculated doses in dogs is two times greater than the variation among measured doses. In most cases,

the minimum and maximum values for the measured doses are higher than the values based upon the calculations.

Table 3.14 Client Owned Dogs Data: Median values and 95% confidence limits of the ratios of ranges, minimums, and maximums values of measured and acalc doses

	Median	95% Confidence Limits	p-value*
Range measured/Range acalc	**0.44**	**0.07 - 1.44**	**0.042**
Min measured/ Min acalc	**1.33**	**0.95 - 2.32**	**0.002**
Max measured/ Max acalc	**1.16**	**0.76 - 1.76**	**0.0322**
Range measured (cGy)	**49.2**	**2.7 - 102.7**	
Range acalc (cGy)	**88.6**	**34.1 - 232.2**	

All reported p-values are by the use of signed rank test because data distribution is not normal

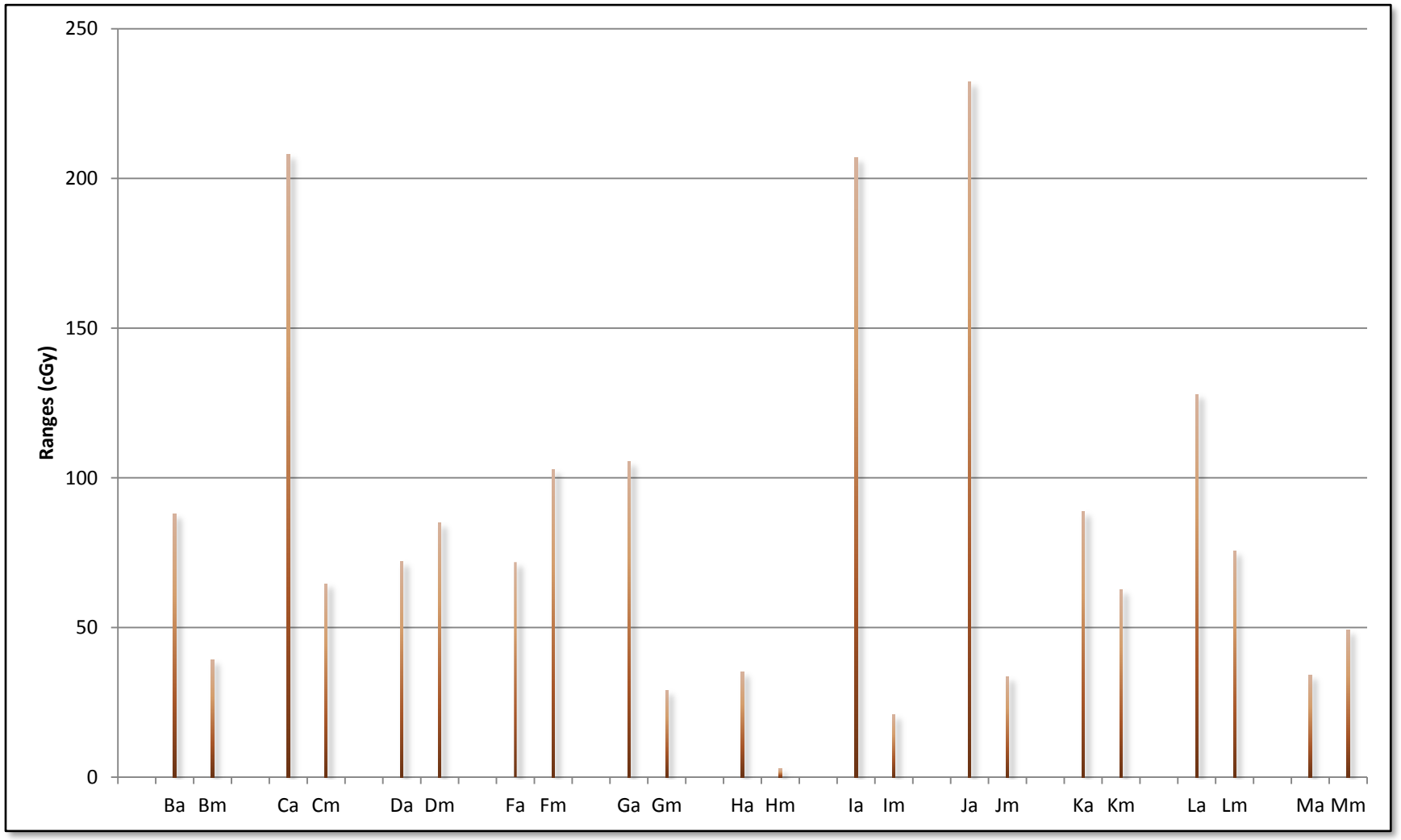

a: average calculated dose *m: measured dose for each dog*

Figure 3.4D Range of measured doses compared to range of average calculated doses in each dog exposure

CHAPTER FOUR

DISCUSSION

4.1 Clinical Cases

At initial presentation, the median age of the participating dogs was 10 years with a range of 5 to 12 years. This is the same median age reported by other investigators.[1,2,4,6] Despite a small sample size, the male to female ratio of 1.6:1 compares favorably to the previously reported ratio of 1.3:1.[3] In the present study, tumors of epithelial origin accounted for 85 % of the cases, which is higher than previously reported but in keeping with the increased incidence of carcinomas in comparison to sarcomas of the nasal cavity.[1-3] Based upon CT, most tumors were found to be unilateral within the nasal cavity, involving predominately the right side. Local invasion of the cribriform plate was reported nearly in one-third of all cases, consistent with the well-known behavior of canine nasal tumors to locally invade surrounding structures. The small sample size of the participating dogs affected the power to evaluate trends thus a larger sample size is recommended.

Since the aim of this study was to characterize dose delivered to oral mucosa during the treatment of canine nasal tumors with SRT, it was critical to track patients after treatment to report the occurrence of radiation-induced

adverse effects, and correlate clinical findings with measured and calculated doses. Table 3.2 lists all the dogs that were followed for the development of adverse effects with their grades according to the VRTOG scoring system. More than half of the dogs developed appreciable acute side effects. All skin reactions were grade I. Mucosal adverse effects were equally divided between grade I and II. Ocular complications were mostly grade II with only one grade III. One dog, known to have ocular changes suggestive of cataract found on the pretreatment ocular exam, developed a cataract several weeks after being treated with radiation. This complication was considered a grade II chronic radiation-induced adverse effect to the eye. All follow-up data was collected by evaluating the CSU ACC medical records. Given that owners are well-educated by the CSU-ACC radiation oncology staff about the possibility of developing radiation-induced adverse effects, and the ways to manage minor complications, some self-limiting adverse effects (especially lower grades) may not be represented within the medical records. Thus, it is probable that minor, self-limiting side effects, not requiring medical attention (i.e. grade I and to a lesser extent grade II adverse effects) are underrepresented within the data. Adverse ocular effects were more profound. The close proximity of the eyes to the nasal cavity makes it harder to spare the eyes during treatment.[14] While outside the focus of this project, additional information is needed regarding ocular toxicity following nasal SRT. Further investigation with a larger sample size over a longer period of time with a focus upon collecting follow up data is recommended to compare the SRT treatment protocol for canine nasal tumors to other radiation protocols regarding toxicity.[20]

4.2 Results from Film System Commissioning

The aim of commissioning EBT film and FilmQA software used in analysis was to provide enough confidence in using them for dose measurements.

4.2A Results from Verifying Step-Wedge Plan Dose

Comparing ion chamber readings to doses calculated by Eclipse and delivered as 13 steps resulted in a less than one percent difference between measured and calculated doses. Thus, there is confidence the accuracy of dose delivery.

4.2B results from Precision Validation of EBT Film and Film Analysis Software

Comparing six calibration curves created from six SW films exposed on separate days resulted in minor difference across the six curves (Table 3.4), these differences tend to increase as applied dose increases. This increase can be attributed to reduced sensitivity within the red channel at doses greater than 4 Gy saturating at doses above 8 Gy.[51] This test provided strong evidence of the precision of the film system, with regard to measuring doses.

4.2C Results from Dose Escalation Validation of EBT film and Film Analysis Software

As seen in figure 3.2C, EBT film demonstrated an overestimation of doses at low doses, while a slope of around 89 cGy (0.89 Gy) suggested a decreasing ability of film to accurately measure doses as they increase. Applying higher dose, increases

the dose lag between applied and measured doses. Plotting the corresponding doses calculated by Eclipse required a more complex model (4th order polynomial curve) depicting the complexity the Eclipse has in predicting these doses. This test proved the sensitivity of EBT film in measuring differing levels of radiation doses with a high degree of accuracy.

4.3 Results of Phantom Data Analysis

Comparing measured doses from the phantom to both doses calculated at reference points (pcalc) and to average doses (aclac) revealed a poor correlation between measured and calculated doses. While there was a statistically significant underestimation of the calculated doses predicted by the Varian Eclipse, there was also a high degree of variability (Table 4.1). Using the average calculated doses neither decreased the degree of variation nor improved the correlation between measured and calculated doses. However, this analysis demonstrated that the mean measured dose was significantly higher than the mean calculated dose in the magnitude of 100 cGy / fraction of SRT.

Table 4.1 Phantom Data: Comparing results from analyzing measured doses to calculated doses at points (pcalc) and to average calculated doses (acalc)

Method	Spearman rank correlation test r/ p-value	Difference Mean (cGy)	Difference STD (cGy)	p-value calculated by use of Paired t-test
Point-to-point comparison	0.016 0.9	112.7	109.5	<0.0001
Point-to-average comparison	-0.06 0.7	103.7	102.7	<0.0001

Another approach was adopted to analyze data by comparing each measured dose point to the range of doses (from minimum to maximum) across the corresponding calculated sphere. All measured points were within the calculated ranges, with a majority of points in the third quartile of the range. The dose interval that contains the majority (89%) of measured points is 488-643.6 cGy/ fraction, while the interval of 410-707cGy/ fraction contains all measured dose points. Calculated doses at reference points (pcalc) have a wider interval where 80% lay between 332.3 and 565.8 cGy, while all points are found in the interval between 176.7 and 721.5 cGy (Fig 4.3.2). This again shows that the Eclipse algorithm underestimates radiation dose delivered to oral mucosa while treating canine nasal tumors with SRT.

To address the concern about high variability between measured and calculated doses, a comparison between measured and average calculated ranges, maximums, and minimums was performed for each phantom exposure in an effort to characterize the amount of variation present (Fig 4.3.1). The range of measured doses was found to be significantly smaller than those of calculated with a median ratio of (0.16:1) and p-value of <0.0001. The minimum measured dose was found to be significantly higher than the minimum calculated dose with a median ratio of (1.26:1) and p-value of 0.0026, while the maximum measured dose was lower than that calculated with a median ratio of (0.936:1) and p-value of 0.0302. These results prove that Eclipse calculations have around six times more variability than the FilmQA measurements. The minimum calculated doses are, typically, smaller than measured, while the maximum calculated doses are slightly higher than the

measured doses. This suggests that when calculated doses are low, there is a greater variation and uncertainty.

Comparison of the median of the measured dose ranges (13.4 cGy) (which is a tight range due to fact that all films were placed within the same spot in each phantom exposure) to median of the calculated dose ranges (95.17 cGy) (which is a wide range), reflects the variation Eclipse has in predicting doses even in points that are few millimeters apart.

Overall the analysis of the phantom data suggests that the Eclipse calculated dose is on average lower than actual delivered dose. Furthermore, the variation makes it difficult to characterize or predict the difference between measured and calculated doses based on individual exposures.

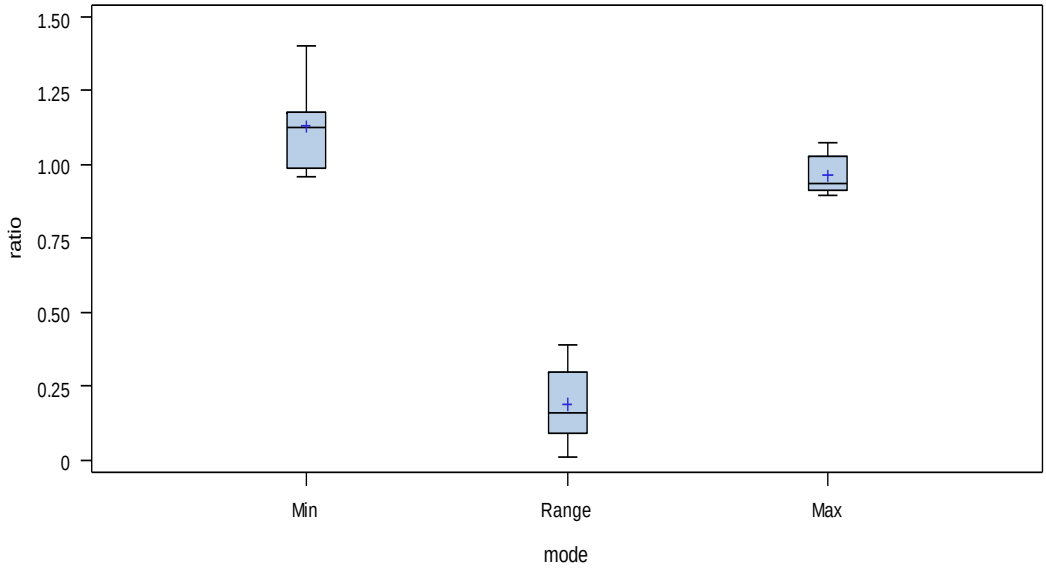

Figure 4.3.1 Box plots showing ratio of measured over average calculated doses for ranges, minimums, and maximums

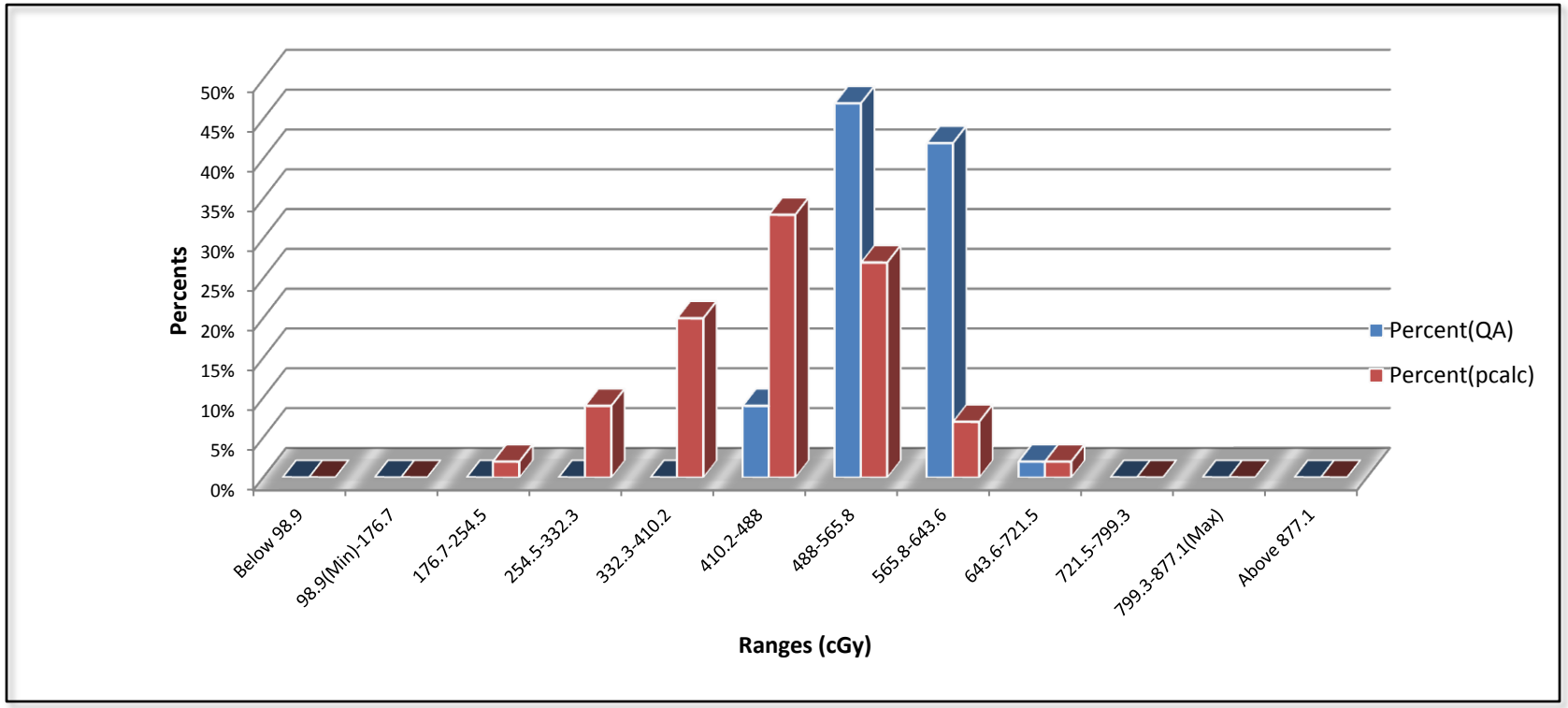

Figure 4.3.2 Measured (QA) and calculated (pcalc) doses relation to the ranges of calculated doses of phantom in cGy

4.4 Results of Dogs Data Analysis

The same analysis approaches applied to the phantom data were applied to the data collected from dogs undergoing SRT for their nasal tumors. Comparing measured doses to both calculated doses at reference points (pcalc) and to average calculated doses (acalc) across the spheres (Table 4.2) revealed a significant positive correlation. Even the use of average calculated dose could not address the issue of high variability. Once again Eclipse underestimated the measured doses to the oral mucosa by about 70 cGy in each delivered fraction.

Table 4.2 Client Owned Dogs: Results from analyzing measured doses to calculated doses at points (pcalc) and to average calculated doses (acalc)

Method	Spearman rank correlation test r/ p-value	Difference Mean (cGy)	Difference STD (cGy)	p-value calculated by use of Wilcoxon two-sample exact test
Point-to-point comparison	**0.44** **0.0024**	**64.4**	**119.2**	**9.2×10^{-5}**
Point-to-average comparison	**0.45** **0.0016**	**74**	**111.2**	**4.2×10^{-5}**

Evaluating the distribution of measured points within the range of calculated doses, in an approach similar to that used with phantom data, reveals that almost all measured point doses were within the range of calculations with the exception of one point where the measured dose exceeded the maximum dose of the calculated range by about 3% (Fig 3.4C.1). The majority (88%) of measured dose points were found to be in the upper half of the calculated range (Fig 4.4.2). In terms of absolute dose this range corresponds to an interval of 356.6-637.5 cGy. Distribution of

calculated doses at reference points (pcalc) has a more pointed peak with a majority of the calculated points (85%) within the central third of the ranges equating to a dose interval of 300- 469 cGy. Additionally the distribution of calculated doses appears to be more skewed toward lower doses as compared to the distribution of measured doses that appears more normal with a tendency toward higher doses. So clinicians should consider, in 88% of the cases evaluated in this study, a dose range anywhere from 3.5 to 6.5 Gy in each fraction delivered to oral mucosa while treating canine nasal tumors with SRT. 10% of the cases receive less than 3.5 Gy per fraction and 2% greater than 6.5 Gy per fraction. The difference between measured and calculated dose cannot be accurately estimated because of the high variability Eclipse demonstrates.

To better characterize the variation between Eclipse calculations and film measurements, ratios of ranges, minimums, and maximums of both groups were considered. This approach revealed a median ratio of measured ranges to calculated ranges of about 0.44, demonstrating that the variation among measured doses was significantly smaller than that of calculated doses with a p-value of 0.042. The median ratio of minimum measurements to minimum calculations was 1.33 (p-value=0.002), proving that the lower end of measured doses are significantly higher than the lower end of calculated doses. While the median ratio of maximum measured doses to maximum calculated doses is 1.165 that also shows that the upper end of measured doses exceeds the upper end of calculated doses (p-value=0.0322). The aforementioned facts prove higher variability (twice) among calculated doses as compared to variability among measured doses particularly at

lower calculated doses (Figure 4.4.1). The median of measured doses ranges was 49.2 cGy, which can be attributed to inter-fractional film positioning variation. The median of calculated doses ranges was 88.6 cGy, which is twice as large as that of measured dose.

The conclusions arising from the analysis of the patient data is close to that reached from analyzing the phantom data. However both the underestimation and variability of the Eclipse calculated doses is less with the patient data.

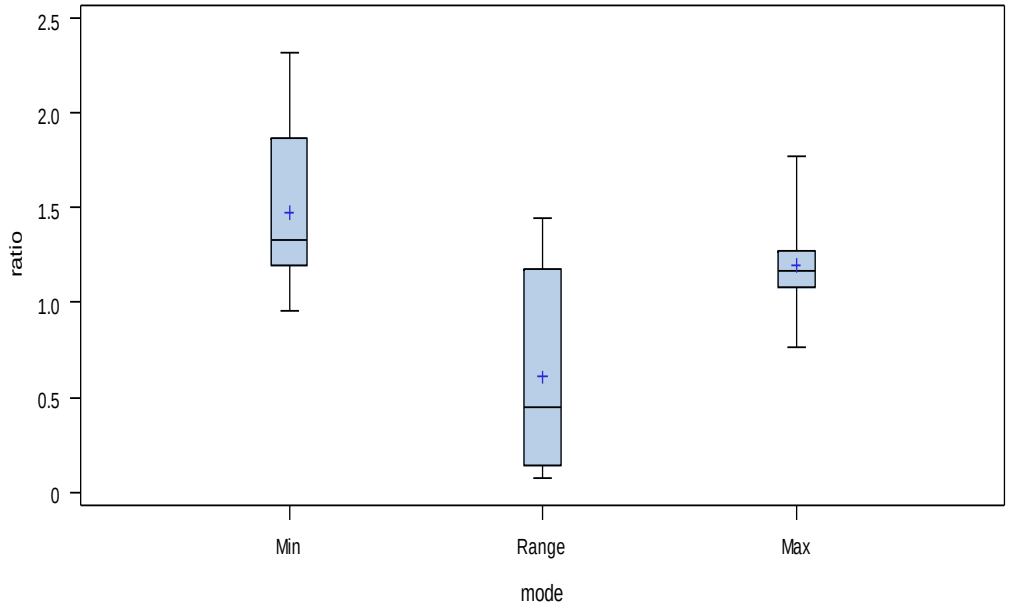

Figure 4.4.1 Box plots showing ratio of measured over average calculated doses for ranges, minimums, and maximums

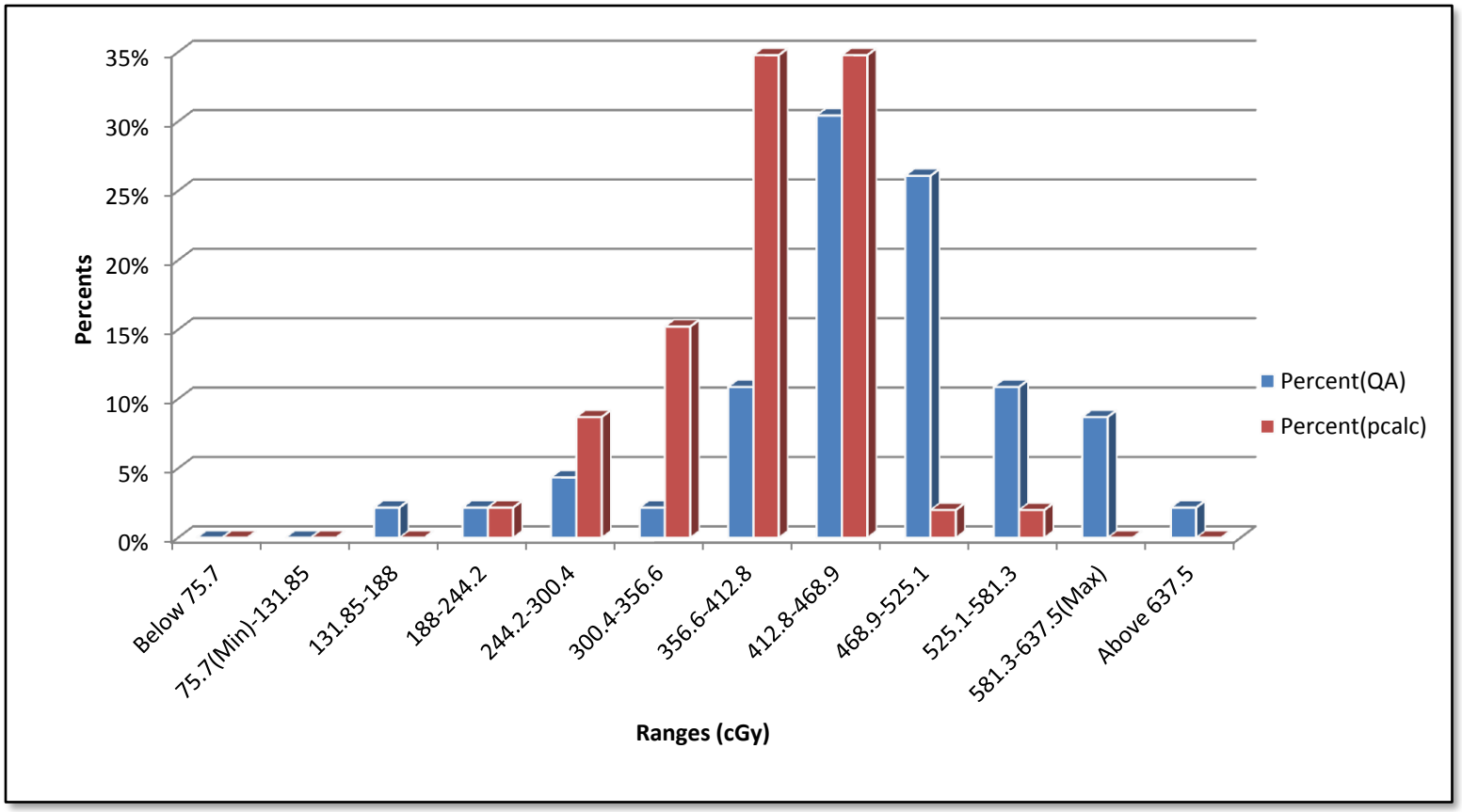

Figure 4.4.2 Measured (QA) and calculated (pcalc) doses relation to the ranges of calculated doses of dogs in cGy

4.5 Comparing Results from Phantom to Actual Patients

The correlation between measured and calculated doses in the patient data was improved as compared to data taken from the phantom exposures. This can be attributed to the minimal variation in measured doses in phantom due to consistent film placement, whereas the measured doses in the dogs varied more due to variations in inter-fractional film positioning. All analyses of differences between the measured and corresponding calculated doses show a tendency of the measured doses to exceed calculated doses by 70 to 100 cGy on average for a 1000 cGy single fraction dose. However the variation was so high for all these comparisons that the above difference cannot be simply applied to all calculations to accurately predict doses to oral mucosa while treating canine nasal tumors with SRT.

Comparing the dose interval for measured dose within the phantom to measured dose for client owned dogs, the phantom data were distributed over a more condensed region (midpoint to 0.7) of the range due to the fact that most of these films were placed within the same spot during each exposure to get more consistent measurements. However ranges from the phantom appear wider than from client owned dogs with a median of (774.2 ± 44.5 compared to 561.8 ± 99.7) cGy, this can be caused by the absence of anatomical rugae in the phantom which obliterated the air gaps between film and mucosa, these air gaps facilitate visualization and identification of the film from underlying tissue in the dogs. However the presence of the air gaps might cause the algorithm to overestimate the impact of the air gap and thus underestimate the dose in this region. For practical

utilization, the dose interval of 356.6 to 637.5 cGy per 10 Gy fraction, where 88% of measurements of real dogs' exposure lay, appear to be more representative and more accurate to be considered by clinicians treating dogs that have nasal tumors with SRT.

Finally, the estimation of variation in calculations compared to measurements using the phantom appears to be higher than the dog data. This can be attributed again to limitations in visualizing the film and delineating it from underlying tissue, it may be a more reasonable estimation of the degree of variability among calculated doses. Due to the fact that measured doses in phantom exposures have a narrow median range (13.4 cGy) compared to (49.2 cGy) in patient exposures, whereas the median range of calculated doses from phantom exposure do not vary much compared to patient exposures (95.2 to 88.6 cGy), suggests that greater variation in measurements are the cause of reducing the ratio of variability among calculated versus measured doses in client owned dogs data.

4.6 Comparing the study results to similar studies

Several studies were conducted to evaluate the accuracy of the Varian Eclipse Anisotropic Analytical Algorithm (AAA) in predicting doses beyond air-tissue interfaces in a heterogeneous media. The results of the previous work was mixed with some indicating a tendency of AAA to overestimate doses,[67-69] while other studies reported the contrary.[49,70] Kan *et al* 2010, investigated the accuracy of AAA in predicting doses to oral mucosa of patients with nasopharyngeal carcinoma

treated with SRT . An anthropomorphic phantom was constructed to simulate the clinical situation and an overestimation of around 3% was reported. Increases in air cavity size and decreases in the treatment field size are factors that increase the degree of overestimation.[26] Oinam *et al* 2010 compared the accuracy of different algorithms in predicting skin dose in head and neck tumors treated with IMRT[27], and demonstrated a tendency of Eclipse AAA to underestimate dose (average difference -4.7 % ± 9.2 % up to 2 mm beyond the interface especially in the high-dose region as defined as within 1.4 cm beyond PTV. For calculation points beyond the interface or away from the PTV, AAA tends to overestimate the delivered doses. High variability in predicting doses was also a finding of this study. The underestimation of dose at interfaces and the high variability are present both in Oinam et. Al. and our work to date.

4.7 Future Work

Accurate estimation of the dose to the oral mucosa of dogs with nasal tumors treated with Varian Eclipse treatment planning software based SRT is not feasible at this time due to the high variability in predicted dose. Further work will be focused on the relationship of different parameters upon the behavior of calculated doses and the resulting variation. PTV volume, distance between PTV margin and oral mucosa, oral cavity volume, dose prescription, and the number of fields are examples of the parameters within dose calculation warranting further investigation. Additional phantom exposures and canine patients could also be pursued in an effort to strengthen existing data.

4.8 Conclusion

The results of this study demonstrate a well-defined difference between measured and AAA calculated dose was difficult to report due to the high degree of variability within the algorithm. Based on the efforts and collected data to date, a dose range of 3.5-6.5 Gy per fraction is to be considered as a more representative estimation of the actual dose delivered to the oral mucosa of a dog treated with nasal SRT, with the exception of tumor invasion to oral mucosa and PTV expansion. This dose interval does not exceed the skin constraints suggested by The American Association of Physicists in Medicine (AAPM) task group 101.[71] However this report was addressing human patients being treated with Stereotactic Body Radiation Therapy (SBRT).

Overall the protocol adopted by Colorado State University-Animal Cancer Center (CSU-ACC) to treat canine nasal tumors with SRT is very well-tolerated by patients and clients. The radiation-induced adverse effects to oral mucosa are minimal even with the proven underestimation of the Varian Eclipse Anisotropic Analytical Algorithm (AAA) to delivered radiation doses. Most dogs with nasal tumors die of failure to achieve local tumor control. Accurately estimating dose to the oral mucosa allows clinicians to feel better about pursuing dose escalation and simultaneous integrated boost to the adjacent tumor. Acknowledgement of the normal tissue tolerance and an ability to accurately predict dose received to normal tissues results in the ability to improve tumor control without increasing the probability of an adverse event.

REFERENCES

1. Turek, M. M., & Lana, S. E. (2007). Canine Nasosinal Tumors. In J. W. Stephen, Dvm, Dacvs, Dacvim & M. V. David (Eds.), *Withrow & MacEwen's Small Animal Clinical Oncology (Fourth Edition)* (pp. 525-539). Saint Louis: W.B. Saunders.
2. Fox, L. E., & King, R. R. (2002). Cancers of the Respiratory System. In W. B. Morrison (Ed.), *Cancer in dogs and cats medical and surgical management* (pp. 497-502). Jackson, Wyo.: Teton NewMedia.
3. Wilson, D. W., & Dungworth, D. L. (2002). Tumors of the Respiratory Tract. In D. J. Meuten (Ed.), *Tumors in domestic animals* (pp. 365-373). Ames, Iowa: Iowa State University Press.
4. McEntee, M. C. (2004). Neoplasms of the Nasal Cavity. In L. G. King (Ed.), *Textbook of respiratory disease in dogs and cats* (pp. 293-301). St. Louis: W.B. Saunders.
5. Venker-van Haagen, A. J. (2005). Tumors of the Nasal plane, the Nasal cavity, and the frontal sinus. In A. J. Venker-van Haagen (Ed.), *Ear, nose, throat, and tracheobronchial diseases in dogs and cats*. Hannover: Schlütersche.
6. Moore, A. S., & Ogilvie, G. K. (2006). Tumors of the Respiratory Tract. In G. K. Ogilvie & A. S. Moore (Eds.), *Managing the canine cancer patient a practical guide to compassionate care* (pp. 405-411). Yardley, PA: Veterinary Learning Systems.
7. Elliot, K. M., & Mayer, M. N. (2009). Radiation therapy for tumors of the nasal cavity and paranasal sinuses in dogs. *Can Vet J, 50*(3), 309-312.
8. McEntee, M. C. (2004). A survey of veterinary radiation facilities in the United States during 2001. *Vet Radiol Ultrasound, 45*(5), 476-479.
9. Rassnick, K. M., Goldkamp, C. E., Erb, H. N., Scrivani, P. V., Njaa, B. L., Gieger, T. L., et al. (2006). Evaluation of factors associated with survival in dogs with untreated nasal carcinomas: 139 cases (1993-2003). *J Am Vet Med Assoc, 229*(3), 401-406.
10. Bommarito, D. A., Kent, M. S., Selting, K. A., Henry, C. J., & Lattimer, J. C. (2011). Reirradiation of recurrent canine nasal tumors. *Vet Radiol Ultrasound, 52*(2), 207-212.
11. Adams, W. M., Bjorling, D. E., McAnulty, J. E., Green, E. M., Forrest, L. J., & Vail, D. M. (2005). Outcome of accelerated radiotherapy alone or accelerated radiotherapy followed by exenteration of the nasal cavity in dogs with intranasal neoplasia: 53 cases (1990-2002). *J Am Vet Med Assoc, 227*(6), 936-941.
12. Adams, W. M., Miller, P. E., Vail, D. M., Forrest, L. J., & MacEwen, E. G. (1998). An accelerated technique for irradiation of malignant canine nasal and paranasal sinus tumors. *Vet Radiol Ultrasound, 39*(5), 475-481.
13. Adams, W. M., Withrow, S. J., Walshaw, R., Turrell, J. M., Evans, S. M., Walker, M. A., et al. (1987). Radiotherapy of malignant nasal tumors in 67 dogs. *J Am Vet Med Assoc, 191*(3), 311-315.

14. Hunley, D. W., Mauldin, G. N., Shiomitsu, K., & Mauldin, G. E. (2010). Clinical outcome in dogs with nasal tumors treated with intensity-modulated radiation therapy. *Can Vet J, 51*(3), 293-300.
15. Lana, S. E., Dernell, W. S., Lafferty, M. H., Withrow, S. J., & LaRue, S. M. (2004). Use of radiation and a slow-release cisplatin formulation for treatment of canine nasal tumors. *Vet Radiol Ultrasound, 45*(6), 577-581.
16. McEntee, M. C., Page, R. L., Heidner, G. L., Cline, J. M., & Thrall, D. E. (1991). A retrospective study of 27 dogs with intranasal neoplasms treated with cobalt radiation. *Veterinary Radiology, 32*(3), 135-139.
17. Mellanby, R. J., Stevenson, R. K., Herrtage, M. E., White, R. A., & Dobson, J. M. (2002). Long-term outcome of 56 dogs with nasal tumours treated with four doses of radiation at intervals of seven days. *Vet Rec, 151*(9), 253-257.
18. Northrup, N. C., Etue, S. M., Ruslander, D. M., Rassnick, K. M., Hutto, D. L., Bengtson, A., et al. (2001). Retrospective study of orthovoltage radiation therapy for nasal tumors in 42 dogs. *J Vet Intern Med, 15*(3), 183-189.
19. Theon, A. P., Madewell, B. R., Harb, M. F., & Dungworth, D. L. (1993). Megavoltage irradiation of neoplasms of the nasal and paranasal cavities in 77 dogs. *J Am Vet Med Assoc, 202*(9), 1469-1475.
20. Custis, J. T., Harmon, J. F., Ryan, S. D., Kraft, S. L., & Larue, S. M. (2011). Canine nasal tumors: a stereotactic radiation therapy approach. [meeting abstract]. *Journal of Veterinary Internal Medicine, 25*(3), 746-747.
21. LaRue, S. M., & Gillette, E. L. (2007). Radiation Therapy. In J. W. Stephen, Dvm, Dacvs, Dacvim & M. V. David (Eds.), *Withrow & MacEwen's Small Animal Clinical Oncology (Fourth Edition)* (pp. 193-210). Saint Louis: W.B. Saunders.
22. Timmerman, R. D., Kavanagh, B. D., Cho, L. C., Papiez, L., & Xing, L. (2007). Stereotactic body radiation therapy in multiple organ sites. *J Clin Oncol, 25*(8), 947-952.
23. Gavin, P. R. (1997). Future of veterinary radiation oncology. *Vet Clin North Am Small Anim Pract, 27*(1), 157-165.
24. Gordon, I. K., & Kent, M. S. (2008). Veterinary radiation oncology: technology, imaging, intervention and future applications. *Cancer Therapy 6*, 167-176.
25. Smith, B. J. (1999). The Oral cavity, Pharynx, Larynx, and Associated Structures. In B. J. Smith (Ed.), *Canine anatomy* (pp. 127). Philadelphia: Williams & Wilkins.
26. Kan, M. W., Cheung, J. Y., Leung, L. H., Lau, B. M., & Yu, P. K. (2011). The accuracy of dose calculations by anisotropic analytical algorithms for stereotactic radiotherapy in nasopharyngeal carcinoma. *Phys Med Biol, 56*(2), 397-413.
27. Oinam, A. S., & Singh, L. (2010). Verification of IMRT dose calculations using AAA and PBC algorithms in dose buildup regions. *J Appl Clin Med Phys, 11*(4), 3351.

28. Fogliata, A., Vanetti, E., Albers, D., Brink, C., Clivio, A., Knoos, T., et al. (2007). On the dosimetric behaviour of photon dose calculation algorithms in the presence of simple geometric heterogeneities: comparison with Monte Carlo calculations. *Phys Med Biol, 52*(5), 1363-1385.
29. Thames, H. D., Jr., Withers, H. R., Peters, L. J., & Fletcher, G. H. (1982). Changes in early and late radiation responses with altered dose fractionation: implications for dose-survival relationships. *Int J Radiat Oncol Biol Phys, 8*(2), 219-226.
30. LaDue, T. A., Dodge, R., Page, R. L., Price, G. S., Hauck, M. L., & Thrall, D. E. (1999). Factors influencing survival after radiotherapy of nasal tumors in 130 dogs. *Vet Radiol Ultrasound, 40*(3), 312-317.
31. Moore, A. S., & Ogilvie, G. K. (2006). Radiation Therapy: Properties, Uses, and patient Management. In G. K. Ogilvie & A. S. Moore (Eds.), *Managing the canine cancer patient a practical guide to compassionate care* (pp. 148-162). Yardley, PA: Veterinary Learning Systems.
32. Webb, S. (2003). The physical basis of IMRT and inverse planning. *Br J Radiol, 76*(910), 678-689.
33. Sjogren, R., & Karlsson, M. (1996). Electron contamination in clinical high energy photon beams. *Med Phys, 23*(11), 1873-1881.
34. Haustermans, K., & Withers, H. R. (2004). The biological basis of fractionation. *Rays, 29*(3), 231-236.
35. Pajonk, F., Vlashi, E., & McBride, W. H. (2010). Radiation resistance of cancer stem cells: the 4 R's of radiobiology revisited. *Stem Cells, 28*(4), 639-648.
36. Harmon, J., Van Ufflen, D., & Larue, S. (2009). Assessment of a radiotherapy patient cranial immobilization device using daily on-board kilovoltage imaging. *Vet Radiol Ultrasound, 50*(2), 230-234.
37. Breitman, K., Rathee, S., Newcomb, C., Murray, B., Robinson, D., Field, C., et al. (2007). Experimental validation of the Eclipse AAA algorithm. *J Appl Clin Med Phys, 8*(2), 76-92.
38. Niroomand-Rad, A., Blackwell, C. R., Coursey, B. M., Gall, K. P., Galvin, J. M., McLaughlin, W. L., et al. (1998). AAPM Report No. 63 Radiochromic Film Dosimetry Recommendations of AAPM Radiation Therapy Committee Task Group No. 55. *MEDICAL PHYSICS, 25*(11), 2093-2115.
39. International Specialty Products. Gafchromic® EBT self-developing film for radiotherapy dosimetry. Wayne, NJ: ISP, 2007. Available from http://online1.ispcorp.com/_layouts/Gafchromic/content/products/ebt/pdfs/EBTwhitepaper.pdf
40. Ladue, T., & Klein, M. K. (2001). Toxicity criteria of the veterinary radiation therapy oncology group. *Vet Radiol Ultrasound, 42*(5), 475-476.
41. Lawrence, J. A., Forrest, L. J., Turek, M. M., Miller, P. E., Mackie, T. R., Jaradat, H. A., et al. (2010). Proof of principle of ocular sparing in dogs with sinonasal tumors treated with intensity-modulated radiation therapy. *Vet Radiol Ultrasound, 51*(5), 561-570.

42. Winslow, J. F., Hyer, D. E., Fisher, R. F., Tien, C. J., & Hintenlang, D. E. (2009). Construction of anthropomorphic phantoms for use in dosimetry studies. *J Appl Clin Med Phys, 10*(3), 2986.
43. Devic, S. (2010). Radiochromic film dosimetry: Past, present, and future. *Phys Med*.
44. International Commission on Radiation Units and Measurement. Tissue substitutes in radiation dosimetry and measurement. . Report No. 44. Bethesda, MD:ICRU, 1989.
45. Butson, M. J., Cheung, T., & Yu, P. K. (2006). Weak energy dependence of EBT gafchromic film dose response in the 50 kVp-10 MVp X-ray range. *Appl Radiat Isot, 64*(1), 60-62.
46. Rink, A., Vitkin, I. A., & Jaffray, D. A. (2007). Energy dependence (75 kVp to 18 MV) of radiochromic films assessed using a real-time optical dosimeter. *Med Phys, 34*(2), 458-463.
47. Chiu-Tsao, S. T., Ho, Y., Shankar, R., Wang, L., & Harrison, L. B. (2005). Energy dependence of response of new high sensitivity radiochromic films for megavoltage and kilovoltage radiation energies. *Med Phys, 32*(11), 3350-3354.
48. Lindsay, P., Rink, A., Ruschin, M., & Jaffray, D. (2010). Investigation of energy dependence of EBT and EBT-2 gafchromic film. *Med Phys, 37*(2), 571-576.
49. Walters, J. (2009). Characterization of differences in calculated and actual measured skin doses to canine limbs during stereotactic radiosurgery using gafchromic™ film. Colorado State University, Fort Collins, CO.
50. Fluke Biomedical Company. Plastic Water™. In Radiation management services product catalog. Available from http://www.bqsv.com.tw/t/htm/e/fluke/RO3.pdf
51. Devic, S., Tomic, N., Soares, C. G., & Podgorsak, E. B. (2009). Optimizing the dynamic range extension of a radiochromic film dosimetry system. *Med Phys, 36*(2), 429-437.
52. Devic, S., Seuntjens, J., Sham, E., Podgorsak, E. B., Schmidtlein, C. R., Kirov, A. S., et al. (2005). Precise radiochromic film dosimetry using a flat-bed document scanner. *Med Phys, 32*(7), 2245-2253.
53. Deveau, M. A., Gutierrez, A. N., Mackie, T. R., Tome, W. A., & Forrest, L. J. (2010). Dosimetric impact of daily setup variations during treatment of canine nasal tumors using intensity-modulated radiation therapy. *Vet Radiol Ultrasound, 51*(1), 90-96.
54. Sorcini, B., & Tilikidis, A. (2006). Clinical application of image-guided radiotherapy, IGRT (on the Varian OBI platform). *Cancer Radiotherapy, 10*(5), 252-257.
55. Chung, H., Lynch, B., & Samant, S. (2010). High-precision GAFCHROMIC EBT film-based absolute clinical dosimetry using a standard flatbed scanner without the use of a scanner non-uniformity correction. *J Appl Clin Med Phys, 11*(2), 3112.

56. JEONG, H. S., HAN, Y., KUM, O., KIM, C. H., JU, S. G., SHIN, J. S., et al. (2010). Pixel-based correction method for gafchromic®EBT film dosimetry. *Nuclear Engineering and Technology, 42*(6), 670-679.
57. Breitman, K., Rathee, S., Newcomb, C., Murray, B., Robinson, D., Field, C., et al. (2007). Experimental validation of the Eclipse AAA algorithm. *J Appl Clin Med Phys, 8*(2), 76-92.
58. Cozzi, L., Nicolini, G., Vanetti, E., Clivio, A., Glashorster, M., Schiefer, H., et al. (2008). Basic dosimetric verification in water of the anisotropic analytical algorithm for Varian, Elekta and Siemens linacs. *Z Med Phys, 18*(2), 128-135.
59. MacEwen, E. G., Withrow, S. J., & Patnaik, A. K. (1977). Nasal tumors in the dog: retrospective evaluation of diagnosis, prognosis, and treatment. *J Am Vet Med Assoc, 170*(1), 45-48.
60. Madewell, B. R., Priester, W. A., Gillette, E. L., & Snyder, S. P. (1976). Neoplasms of the nasal passages and paranasal sinuses in domesticated animals as reported by 13 veterinary colleges. *Am J Vet Res, 37*(7), 851-856.
61. Henry, C. J., Brewer, W. G., Jr., Tyler, J. W., Brawner, W. R., Henderson, R. A., Hankes, G. H., et al. (1998). Survival in dogs with nasal adenocarcinoma: 64 cases (1981-1995). *J Vet Intern Med, 12*(6), 436-439.
62. Laing, E. J., & Binnington, A. G. (1988). Surgical therapy of canine nasal tumors: A retrospective study (1982-1986). *Can Vet J, 29*(10), 809-813.
63. Holmberg, D. L., Fries, C., Cockshutt, J., & Van Pelt, D. (1989). Ventral rhinotomy in the dog and cat. *Vet Surg, 18*(6), 446-449.
64. Hahn, K. A., Knapp, D. W., Richardson, R. C., & Matlock, C. L. (1992). Clinical response of nasal adenocarcinoma to cisplatin chemotherapy in 11 dogs. *J Am Vet Med Assoc, 200*(3), 355-357.
65. Langova, V., Mutsaers, A. J., Phillips, B., & Straw, R. (2004). Treatment of eight dogs with nasal tumours with alternating doses of doxorubicin and carboplatin in conjunction with oral piroxicam. *Aust Vet J, 82*(11), 676-680.
66. Lana, S. E., Dernell, W. S., LaRue, S. M., Lafferty, M. J., Douple, E. B., Brekke, J. H., et al. (1997). Slow release cisplatin combined with radiation for the treatment of canine nasal tumors. *Vet Radiol Ultrasound, 38*(6), 474-478.
67. Murphy, M. J., Balter, J., Balter, S., BenComo, J. A., Das, I. J., Jiang, S. B., et al. (2007). The management of imaging dose during image-guided radiotherapy: Report of the AAPM Task Group 75. *Medical Physics, 34*(10), 4041.
68. Spiers, F. W. (1946). Effective atomic number and energy absorption in tissues. *Br J Radiol, 19*, 52-63.
69. McCullough, E. C., & Holmes, T. W. (1985). Acceptance testing computerized radiation therapy treatment planning systems: direct utilization of CT scan data. *Med Phys, 12*(2), 237-242.
70. Bukowski, J. A., Wartenberg, D., & Goldschmidt, M. (1998). Environmental causes for sinonasal cancers in pet dogs, and their usefulness as sentinels of indoor cancer risk. *J Toxicol Environ Health A, 54*(7), 579-591.

71. Reif, J. S., Bruns, C., & Lower, K. S. (1998). Cancer of the nasal cavity and paranasal sinuses and exposure to environmental tobacco smoke in pet dogs. *Am J Epidemiol, 147*(5), 488-492.